VIBRATION ISOLATION FOR FLEXIBLE SPACE STRUCTURES: ZEROS-BASED AND DECENTRALIZED CONTROL APPROACHES

NAG-1-1418LA

Final Report

Principal Investigator: Trevor W. Williams, Associate Professor
Department of Aerospace Engineering
University of Cincinnati

Technical Monitor: Dr. Peiman Maghami
Spacecraft Controls Branch
NASA Langley Research Center

Abstract

The transmission zeros of a flexible space structure (FSS) depend on the locations at which its sensors and actuators are positioned, and provide a great deal of information concerning the closed-loop performance that is achievable with this sensor/actuator arrangement. Furthermore, the zeros of non-collocated structures possess entirely different properties than those of the zeros of collocated structures. The first part of this report analyzes these properties, and quantifies the extreme sensitivity to sensor and actuator position that can occur for non-collocated zeros.

The report then describes two computationally efficient techniques for the related problem of placing instruments on a flexible structure so as to minimize the disturbance effects of the slewing of one instrument on the pointing performance of the others. In both approaches, perturbation methods are used to derive ideal directions in which each instrument should be displaced so as to reduce some measure of cross-instrument observability as much as possible; the difference between the approaches lies in the details of the observability measure used. The methods are illustrated by application to two structural models, one continuous and the other discrete; both demonstrate the improvement in performance that is achievable by the purely passive technique of repositioning instruments. Furthermore, in the course of this analysis, the degrees of controllability and observability of close structural modes are quantified in detail.

Finally, the report addresses the question of designing efficient decentralized controllers for FSS. One factor which must be borne in mind in this analysis is that the controllability and observability Grammian matrices which are usually studied are inherently open-loop quantities; they therefore do not reflect any decentralized structure present in the controller. In order to overcome this problem, new *closed-loop Grammians* are introduced here, and shown to be very useful for analysis of decentralized FSS controllers. In particular, they lead to a natural technique for performing a sequential loop-closing form of controller design, based on closing single input/single output feedback loops between a set of decentralized sensor and actuator pairs, possibly collocated.

TABLE OF CONTENTS

1. Introduction

The positions at which sensors, actuators and sensitive instruments are placed on flexible space structures (FSS) is crucial to the pointing and tracking results that can then be obtained. For this reason, there has been a considerable amount of work done on this type of problem in the past; see, for instance, References 32, 33, 41 and 42 for recent research on this subject.

In practice, flexible structures must often be controlled by means of non-collocated sensors and actuators. This may be necessary not only so as to avoid the performance limitations inevitable in collocated structures, but also because construction of true collocated sensors and actuators is very difficult to achieve. (The NASA Langley CSI Evolutionary Model is a notable example of a structure which does possess essentially collocated sensors and actuators.) Unfortunately, non-collocation nearly always leads [1] to right half-plane transmission zeros. Furthermore, these zeros have been observed [2][3] to be, in some cases, extremely sensitive to the choice of FSS model order, as well as to the exact positions of sensors and actuators. This contrasts sharply with the collocated case, where the zeros always lie [4] in the left half-plane, and have sensitivities to model order [5] and modal parameters [6] which are comparable to those of the system poles. However, a quantitative explanation of the ill-conditioning of non-collocated zeros has not yet been obtained.

This question is addressed in the next three sections of this report, where it is shown that ill-conditioning occurs when the *zero direction* constrained mode shape [7][8] and its dual are nearly orthogonal. Two new condition numbers are then derived that quantify the sensitivity of the zeros to sensor and actuator position variations, and conclusions drawn concerning the zeros of near-collocated structures. These results are then used to study the difficult non-collocated sensor/actuator placement problem.

The report then describes two computationally efficient techniques for the related problem of placing instruments on a flexible structure so as to minimize the disturbance effects of the slewing of one instrument on the pointing performance of the others. In both approaches, perturbation methods are used to derive ideal directions in which each instrument should be displaced so as to reduce some measure of cross-instrument observability as much as possible; the difference between the approaches lies in the details of the observability measure used. Both versions use the *closed-form Grammians* of flexible structures [16][18] to find analytical expressions for the changes in the *Hankel singular values (HSVs)* of an FSS which occur as a result of a shift in instrument positions. However, one method is based on minimizing the largest of the Hankel singular values, while the other reduces the sum of the HSVs. It will be shown that the the first of these approaches is somewhat more computationally expensive than the second, but also gives more reliable results for certain types of problem. In the process of setting up the two techniques, extensive results will be presented on the *degrees of controllability and observability* of close modes of flexible structures. Such modes arise often in practice, typically as a result of either symmetry or repeated sub-structure elements, and are known to greatly complicate the question of determining the controllability and observability properties of such a structure. The new results presented here address this question in some detail.

The observability perturbations computed using either of these two methods are then used to decide how to shift each instrument in turn so as to minimize cross-instrument interactions. For continuous structures, the orthogonal projection of this optimal shift direction onto the physical structure determines the optimal feasible shift for each instrument. The problem is somewhat more constrained for discrete, truss-like structures: in this case, the optimal shift direction now determines which of the few possible directions of motion is most efficacious. In either case, iterating over all instruments leads to a final set of highly non-interacting instrument locations on the structure. The two variants, i.e. that based on minimizing the maximal HSV and that based on reducing the HSV sum, are illustrated in Section 9 by application to a uniform simply-supported

plate in the continuous case, and the ASTREX truss structure in the discrete case. Both of these examples demonstrate the improvement in performance that is achievable by the purely passive technique of repositioning instruments, as opposed to an active control scheme.

Finally, it should be noted that the control of flexible space structures (FSS) is often analyzed in a centralized framework, where the outputs of all sensors on the structure are fed back to all of the actuators. However, a decentralized arrangement is much more amenable to practical implementation. In this type of system, only a specified subset of sensors (possibly only a single one) is connected to each particular actuator, giving rise to a set of independent local controllers. This constraint on the structure of the feedback gain matrix implies that decentralized controllers will generally possess lower performance than that of a centralized controller. For instance, there may exist closed-loop poles, known as *decentralized fixed modes* (the equivalent of uncontrollable poles in centralized control), which can be shifted by centralized feedback but not by decentralized control. This type of complication should be considered when designing decentralized controllers.

The final part of the report addresses the question of designing efficient decentralized controllers for FSS. One factor which must be borne in mind in this analysis is that the controllability and observability Grammian matrices which are usually studied are inherently open-loop quantities; they therefore do not reflect any decentralized structure present in the controller. In order to overcome this problem, the new *closed-loop Grammians* are introduced here, and shown to be very useful for analysis of decentralized FSS controllers. In particular, they lead to a natural technique for performing a sequential loop-closing form of controller design, based on closing single input/single output feedback loops between a set of decentralized sensor and actuator pairs, possibly collocated.

2. Zeros of Flexible Structures

Consider an n-mode model for the structural dynamics of a modally damped, non-gyroscopic, non-circulatory FSS with m sensors (measuring either rates or displacements) and an equal number of actuators. This model can be written in modal form [9] as

$$\begin{aligned} &\ddot{\boldsymbol{\eta}} + diag(2\zeta_i\omega_i)\dot{\boldsymbol{\eta}} + diag(\omega_i^2)\boldsymbol{\eta} = \Phi_a^T\mathbf{u}, \\ &\mathbf{y} = \Phi_r\dot{\boldsymbol{\eta}} + \Phi_d\boldsymbol{\eta}, \end{aligned} \tag{2.1}$$

where η is the vector of modal coordinates, and Φ_a, Φ_r and Φ_d are the actuator, rate sensor and displacement sensor influence matrices, respectively. ω_i and ζ_i are the natural frequency and damping ratio of the i^{th} mode; for the typical FSS [10], the $\{\zeta_i\}$ are quite low (e.g. 0.005), and the $\{\omega_i\}$ occur in clusters of nearly-repeated frequencies.

Defining the state vector $\mathbf{x} = \left(\dot{\boldsymbol{\eta}}^T, \boldsymbol{\eta}^T\right)^T$ yields the state space model $\dot{\mathbf{x}} = A\mathbf{x} + B\mathbf{u}$, $\mathbf{y} = C\mathbf{x}$ for this structure, where

$$A = \begin{pmatrix} -diag(2\zeta_i\omega_i) & -diag(\omega_i^2) \\ I_n & 0 \end{pmatrix}, B = \begin{pmatrix} \Phi_a^T \\ 0 \end{pmatrix} \text{and } C = \begin{pmatrix} \Phi_r & \Phi_d \end{pmatrix}. \tag{2.2}$$

The *transmission zeros* [35] of this system are those values of s which reduce the rank of its *system matrix*, i.e. those s for which a non-trivial solution exists for the equation

$$\begin{pmatrix} sI_{2n} - A & B \\ C & 0 \end{pmatrix} \begin{pmatrix} \mathbf{x}(s) \\ -\mathbf{u}(s) \end{pmatrix} = \mathbf{0}. \tag{2.3}$$

This can clearly be put in the form of a *generalized eigenvalue problem*

$$\hat{A}\mathbf{p} = \lambda\hat{B}\mathbf{p}, \tag{2.4}$$

where the generalized eigenvalue is the zero $s = \lambda$, the corresponding generalized eigenvector is $\mathbf{p} = \begin{pmatrix} \mathbf{x}(s)^T & -\mathbf{u}(s)^T \end{pmatrix}^T$, and the matrices $\hat{A}$ and $\hat{B}$ are defined as

$$\hat{A} = \begin{pmatrix} A & -B \\ -C & 0 \end{pmatrix} \text{ and } \hat{B} = \begin{pmatrix} I_{2n} & 0 \\ 0 & 0 \end{pmatrix}. \tag{2.5}$$

The zeros of structures with collocated sensors and actuators can be shown to possess certain desirable properties. For instance, if the structure is undamped they *interlace* [7] the poles along the imaginary axis; if it is damped, the zeros are guaranteed to be stable, lying in a region [4] in the left half-plane which is defined by, and in the vicinity of, the open-loop poles. By contrast, certain of the zeros of a non-collocated structure will generally lie in the right half-plane[1][2], so giving rise to a *non-minimum phase* system with all its attendant control difficulties [35]. Similarly, the zeros of collocated structures are roughly only as sensitive to changes in model order [5] and structural parameters [6] as are its poles; no such guarantees are possible in the non-collocated case. In fact, the higher-frequency zeros of a non-collocated structure are typically extremely sensitive to changes in the assumed model order [2], a practical point of some significance.

3. Effects of Sensor and Actuator Perturbations

The zeros of flexible structures with certain configurations of non-collocated sensors and actuators can also be extremely sensitive [2][3] to small changes in the positions of these sensors and/or actuators. This again contrasts with the collocated case, where the zeros can be shown [8] to be relatively insensitive to small shifts in sensor/actuator location. First-order generalized eigenvalue perturbation methods will now be used to analyze this question, so providing insight into the circumstances under which this type of ill-conditioning can arise.

If the generalized eigenvalue problem (2.4) has left generalized eigenvector $\mathbf{q}$, i.e. the vector satisfying

$$\mathbf{q}^H \hat{A} = \lambda \mathbf{q}^H \hat{B}, \tag{3.1}$$

then a simple approximation can be derived for the generalized eigenvector $\lambda + \delta\lambda$ of the perturbed problem obtained for $\hat{A} \mapsto \hat{A} + \delta\hat{A}$ and $\hat{B} \mapsto \hat{B} + \delta\hat{B}$. Normalizing the left and right eigenvectors of the nominal problem so as to give $\|\mathbf{p}\|_2 = \|\mathbf{q}\|_2 = 1$, then the corresponding eigenvalue of the perturbed problem is [11], to first order,

$$\lambda + \delta\lambda \approx \frac{\mathbf{q}^H(\hat{A} + \delta\hat{A})\mathbf{p}}{\mathbf{q}^H(\hat{B} + \delta\hat{B})\mathbf{p}}. \tag{3.2}$$

In the particular case of sensor and actuator motion on a flexible structure, the appropriate matrix perturbations are, from (2.2) and (2.5),

$$\delta\hat{A} = \begin{pmatrix} 0 & \begin{pmatrix} -\delta\Phi_a^T \\ 0 \end{pmatrix} \\ \begin{pmatrix} -\delta\Phi_r & -\delta\Phi_d \end{pmatrix} & 0 \end{pmatrix} \text{ and } \delta\hat{B} = 0. \tag{3.3}$$

Now, premultiplying (2.4) by $\mathbf{q}^H$ clearly gives $\lambda = \mathbf{q}^H\hat{A}\mathbf{p}/\mathbf{q}^H\hat{B}\mathbf{p}$. This, together with (3.2) and the fact that $\delta\hat{B} = 0$, then yields

$$\delta\lambda \approx \frac{\mathbf{q}^H \delta\hat{A}\mathbf{p}}{\mathbf{q}^H \hat{B}\mathbf{p}}. \tag{3.4}$$

The right generalized eigenvector $\mathbf{p}$ was, from (2.3), of the form $\mathbf{p} = \begin{pmatrix}\mathbf{x}^T & -\mathbf{u}^T\end{pmatrix}^T$. If we write the left eigenvector $\mathbf{q}$ similarly as $\mathbf{q} = \begin{pmatrix}\mathbf{z}^T & -\mathbf{v}^T\end{pmatrix}^T$, where the physical significance of these subvectors will be discussed below, the eigenvalue perturbation can be expanded as

$$\delta\lambda \approx \frac{\mathbf{z}^H\begin{pmatrix}\delta\Phi_a & 0\end{pmatrix}^T\mathbf{u} + \mathbf{v}^H\begin{pmatrix}\delta\Phi_r & \delta\Phi_d\end{pmatrix}\mathbf{x}}{\mathbf{z}^H\mathbf{x}}. \tag{3.5}$$

It is interesting to note the similarity of the denominator of this expression to the *condition number* [12][13] of the standard eigenvalue problem. For, if $A\mathbf{x} = \lambda\mathbf{x}$ and $\mathbf{z}^H A = \mathbf{z}^H\lambda$ with $\|\mathbf{x}\|_2^2 = \|\mathbf{z}\|_2^2 = 1$, then the condition number of λ with respect to perturbations in the matrix A is just $c(\lambda) = 1/|\mathbf{z}^H\mathbf{x}|$, or the secant of the angle between the left and right eigenvectors. The eigenvalue will therefore be ill-conditioned whenever these vectors are nearly orthogonal. Equation (3.5) leads to a very similar observation for the generalized eigenvalue problem (2.4), the main difference being that it is orthogonality of the subvectors $\mathbf{x}$ and $\mathbf{z}$ that will lead to ill-conditioning, not orthogonality of the entire eigenvectors $\mathbf{p}$ and $\mathbf{q}$.

The physical significance of this result can be made clearer by consideration of the structure of the vectors $\mathbf{x}$ and $\mathbf{z}$. If we write these as $\mathbf{x} = \begin{pmatrix}\mathbf{x}_1^T & \mathbf{x}_2^T\end{pmatrix}^T$ and $\mathbf{z} = \begin{pmatrix}\mathbf{z}_1^T & \mathbf{z}_2^T\end{pmatrix}^T$, then (2.2) yields $\lambda\mathbf{x}_2 = \mathbf{x}_1$ and

$$\begin{aligned}&[\lambda^2 I_n + \lambda\cdot diag(2\zeta_i\omega_i) + diag(\omega_i^2)]\mathbf{x}_2 = \Phi_a^T\mathbf{u},\\ &(\lambda\Phi_r + \Phi_d)\mathbf{x}_2 = \mathbf{0}\end{aligned} \tag{3.6}$$

for the right eigenvector. Thus, $\mathbf{x}_2$ is the *constrained mode shape* [7][8], or *zero direction*, associated with the zero λ. This is a forced mode of vibration of the structure which is excited from the actuator stations (equation (3.6[a])), and gives rise to identically zero measured motion at

the sensor stations (the unobservability constraint (3.6b)). Considering the left eigenvector in a similar fashion gives

$$\begin{aligned} &\mathbf{z}_1^H[\lambda^2 I_n + \lambda \cdot diag(2\zeta_i\omega_i) + diag(\omega_i^2)] = \mathbf{v}^H(\lambda\Phi_r + \Phi_d), \\ &\mathbf{z}_1^H\Phi_a^T = \mathbf{0}. \end{aligned} \tag{3.7}$$

$\mathbf{z}_1$ is therefore the constrained mode shape associated with (the complex conjugate of) λ that would be obtained for the *dual* structure which has sensors at the locations of actuators on the physical structure, and actuators at the physical sensor stations. These constrained mode shapes will now be shown to determine, to a large extent, the sensitivity of the zero λ to sensor and actuator perturbations.

Using the fact that $\lambda\mathbf{x}_2 = \mathbf{x}_1$, (3.5) becomes

$$\delta\lambda \approx \frac{\mathbf{z}_1^H\delta\Phi_a^T\mathbf{u} + \mathbf{v}^H(\lambda \cdot \delta\Phi_r + \delta\Phi_d)\mathbf{x}_2}{(\lambda\mathbf{z}_1^H + \mathbf{z}_2^H)\mathbf{x}_2}. \tag{3.8}$$

The denominator of this expression can now be rewritten using the left eigenvector equations to eliminate the subvector $\mathbf{z}_2$. These give $\mathbf{z}_2^H = \mathbf{z}_1^H[\lambda \cdot I_n + diag(2\zeta_i\omega_i)] - \mathbf{v}^H\Phi_r$, so we have

$$\delta\lambda \approx \frac{\mathbf{z}_1^H\delta\Phi_a^T\mathbf{u} + \mathbf{v}^H(\lambda \cdot \delta\Phi_r + \delta\Phi_d)\mathbf{x}_2}{\mathbf{z}_1^H[2\lambda \cdot I_n + diag(2\zeta_i\omega_i)]\mathbf{x}_2 - \mathbf{v}^H\Phi_r\mathbf{x}_2}. \tag{3.9}$$

This expression is particularly simple for undamped structures with no rate outputs, giving

$$\delta\lambda \approx \frac{\mathbf{z}_1^H\delta\Phi_a^T\mathbf{u} + \mathbf{v}^H\delta\Phi_d\mathbf{x}_2}{2\lambda\mathbf{z}_1^H\mathbf{x}_2}. \tag{3.10}$$

The significance of the constrained modes $\mathbf{x}_2$ and $\mathbf{z}_1$ can now be seen: if these vectors are nearly orthogonal, the corresponding zero of the structure will be very sensitive to sensor and/or actuator position changes. We have therefore proved the following result.

Lemma 1: The sensitivity of the zero λ of a flexible structure to actuator position changes is quantified by the condition number $c_a(\lambda) = \|\mathbf{z}_1\|_2 \cdot \|\mathbf{u}\|_2 / 2\lambda |\mathbf{z}_1^T \mathbf{x}_2|$; the corresponding condition number with respect to displacement sensor position is $c_d(\lambda) = \|\mathbf{x}_2\|_2 \cdot \|\mathbf{v}\|_2 / 2\lambda |\mathbf{z}_1^T \mathbf{x}_2|$.

Proof: By the properties of matrix norms we have $|\delta\lambda| \le c_a(\lambda) \cdot \|\delta\Phi_a\|_2 + c_d(\lambda) \cdot \|\delta\Phi_d\|_2$, which is of the upper bound form desired for condition numbers.

As noted previously, the zeros of collocated structures are generally far less sensitive to sensor/actuator placement errors than are those of non-collocated structures. This can now be proved from the preceding analysis. (Note that both $\mathbf{z}_1$ and $\mathbf{v}$ are purely real for such systems, so conjugate transposes are replaced by transposes below.)

Lemma 2: A zero λ of a collocated structure has condition number with respect to both sensor and actuator positions given by $c_c(\lambda) = \|\mathbf{u}\|_2 \cdot \|\mathbf{x}_2\|_2 / 2\lambda \|\mathbf{x}_2\|_2^2 = \|\mathbf{u}\|_2 / 2\lambda \|\mathbf{x}_2\|_2$, the denominator of which is always non-zero for any $\lambda \neq 0$.

Proof: This follows from setting $\Phi_d = \Phi_a$, which gives $\mathbf{z}_1 = \mathbf{x}_2$ and $\mathbf{v} = \mathbf{u}$, so reducing (3.10) to

$$\delta\lambda \approx \frac{\mathbf{x}_2^T \delta\Phi_a^T \mathbf{u} + \mathbf{u}^T \delta\Phi_d \mathbf{x}_2}{2\lambda \mathbf{x}_2^T \mathbf{x}_2} = \frac{\mathbf{u}^T (\delta\Phi_a + \delta\Phi_d)\mathbf{x}_2}{2\lambda \|\mathbf{x}_2\|_2^2}. \tag{3.11}$$

This result is analogous to the fact that the left and right eigenvectors of symmetric matrices are equal, and so the eigenvalues of such matrices are never ill-conditioned [12][13].

Another fundamental result concerning collocated undamped structures is that their zeros are always [7][4] purely imaginary. This is turn now implies the following. (A similar result also holds for structures with near-collocated actuators and rate sensors.)

Lemma 3: The zeros of a structure with near-collocated actuators and displacement sensors are, to first order, purely imaginary.

Proof: Taking $\lambda = j\omega_z$ in (3.11), we have

$$\delta\lambda \approx -j \cdot \frac{\mathbf{u}^T(\delta\Phi_a + \delta\Phi_d)\mathbf{x}_2}{2\omega_z \|\mathbf{x}_2\|_2^2}, \tag{3.12}$$

which is also purely imaginary.

The sensitivity of the zeros to actuator and sensor positioning can have direct consequences for the sensitivity of the closed-loop poles obtained for this system. Consider, for instance, the case of output feedback

$$\mathbf{u} = -K\mathbf{y}. \tag{3.13}$$

The resulting closed-loop system has state matrix $\hat{A} = A - BKC$, the eigenvalues of which are the closed-loop poles. Let $\hat{\mathbf{x}}$ and $\hat{\mathbf{z}}$ be the normalized right and left eigenvectors, respectively, corresponding to a closed-loop pole $\hat{\lambda}$. Then, the first-order perturbation of $\hat{\lambda}$ with respect to a change in B (due to a shift in actuator position) is just [12][13]

$$\delta\hat{\lambda} \approx -\frac{\hat{\mathbf{z}}^H \delta BKC\hat{\mathbf{x}}}{\hat{\mathbf{z}}^H\hat{\mathbf{x}}}. \tag{3.14}$$

But $-KC\hat{\mathbf{x}}$ is just the control input $\hat{\mathbf{u}}$ required to excite the closed-loop system at this mode, and (by (2.2)) $\delta B = \begin{pmatrix}\delta\Phi_a & 0\end{pmatrix}^T$. Thus, (3.14) can be rewritten as

$$\delta\hat{\lambda} \approx \frac{\hat{\mathbf{z}}^H \begin{pmatrix}\delta\Phi_a & 0\end{pmatrix}^T \hat{\mathbf{u}}}{\hat{\mathbf{z}}^H\hat{\mathbf{x}}}. \tag{3.15}$$

If K is sufficiently large that the closed-loop pole $\hat{\lambda}$ is approximately equal to a zero, λ, of the system, then the corresponding left and right closed-loop mode shapes $\hat{\mathbf{z}}$ and $\hat{\mathbf{x}}$ will be approximately equal to the corresponding left and right zero directions, $\mathbf{z}$ and $\mathbf{x}$ respectively. Thus, comparing (3.15) with (3.5) reveals that, in the high-gain case, the sensitivity of a closed-loop pole to shifts in actuator location is asymptotically equal to that of the zero it is approaching. This logical result will be illustrated graphically in the next section.

Finally, it should be noted that the zero perturbation results obtained above can also be used for the difficult problem of non-collocated sensor/actuator placement. A practical objective [32][33] is to shift sensors and/or actuators so as to make the resulting zeros as damped as possible, i.e. so that their real parts are as large and negative as possible. In this way, the closed-loop poles obtained by applying output feedback or optimal state feedback [35] will be heavily damped, giving fast closed-loop response regulation. Considering an undamped structure with displacement sensors for simplicity, it can be seen from (3.10) that the effect on the zero λ of shifting the i^{th} actuator by an amount $\delta\mathbf{b}_i$ (as yet unspecified) is to contribute a term

$$\delta\lambda \approx \frac{\mathbf{z}_1^H \delta\mathbf{b}_i u_i}{2\lambda \mathbf{z}_1^H \mathbf{x}_2} \equiv \mathbf{r}^H \delta\mathbf{b}_i, \tag{3.16}$$

where u_i is the i^{th} entry of $\mathbf{u}$. This will have the desired result if the real vector $\delta\mathbf{b}_i$ is chosen so as to be as nearly as possible anti-parallel to the known vector $\text{Re}(\mathbf{r})$, a simple condition to apply. Similar results clearly also hold for sensor placement.

4. Zeros Sensitivity Results

In order to investigate the properties of non-collocated zeros in detail, consider the particular case of a uniform cantilever beam. The dimensions of this beam will be taken to be length 25 m, width 0.1 m and depth 0.01 m, and its material properties those of aluminum (density 2.7×10^3 kg/m^3, Young's modulus 7.0×10^{10} N/m^2). A single force actuator is located at the free tip of the beam, and a linear displacement sensor moved along its entire length, i.e. through all normalized lengths p, $0 \leq p \leq 1$. Many of the resulting transmission zeros are found to occur in positive/negative real or imaginary pairs, as is the case for distributed parameter models. However, there also exist general **complex** zeros, with these occurring in quadruples symmetric about the real and imaginary axes. These complex zeros, the existence of which is not suggested from distributed models, are illustrated in Figs. 4.1 and 4.2 for beam models of orders 6 and 7, respectively.

Although the behavior represented by these *zero locus* diagrams is quite complicated, the general trends can be summarized fairly simply. For p near 0 (sensor near the built-in end of the beam), the complex zeros depart the two terminating points on the right-hand side of the figures; there is also a real zero pair near the origin. As p increases, the smaller complex zero moves towards the real axis fairly directly, while the other travels towards the real axis in loops, reaching it towards the left-hand side of the figures. The remaining arcs (one in Fig. 4.1; two in Fig. 4.2) are caused by real zeros which approach the origin for moderate p values, split into complex quadruples, and then become real once more. Finally, as p approaches unity (the collocated case), the zeros migrate out along the real axes and then in along the imaginary axes, taking up the interlaced collocated values.

The complex zeros are very sensitive to the choice made for model order; this can be seen from the fact that Figs. 4.1 and 4.2 do not overlap to any great extent. The zeros can also be extremely sensitive to sensor and/or actuator position. For instance, there are quite large gaps in the vicinity of the loops in the figures, despite the fact that they were plotted for a step size in p of 0.002, i.e. a

sensor position increment of 0.05 m. Fig. 4.3 shows the subplot for n = 6 and p between 0.20 and 0.21; the sensor position step used is now 5 mm. Superimposed on the figure are the corresponding zeros condition numbers as computed by the method described above. The larger-magnitude zeros, i.e. the complex zeros and the larger real ones, can be observed to be moving quite rapidly in this diagram, and so are extremely sensitive to changes in p. Comparing these values with those obtained for a portion of the locus where the zeros are not so mobile (Fig. 4.4; p between 0.30 and 0.31) shows nearly a hundredfold change in the zeros condition numbers. The new condition number definition has therefore allowed this zeros sensitivity to be quantified precisely.

A further illustration of the sensitivity of the zeros is provided by the *zeros sensitivity profile* of the beam. This is a plot of the average condition number of all the zeros of the structure as a function of actuator normalized position p. Figure 4.5 gives such a plot for the case of a 6-mode beam model, and Figure 4.6 gives the corresponding plot for $n = 7$. It can be seen that the main feature is a system of $(n - 1)$ nearly equally spaced peaks of extremely high amplitude, where one or other zeros becomes extremely sensitive to actuator position. This can be explained in terms of the condition number analysis given previously, i.e. ill-conditioning arises when the appropriate left and right eigenvectors become orthogonal. Alternatively, a wave equation formulation [34] may possible lead to insight into where extreme ill-conditioning arises, and to explain why this occurs for nearly equally spaced locations. It should also be noted from the subplots that less severe ill-conditioning is also observed for other actuator positions, for instance $p = 0.29$ for $n = 7$. The wealth of information provided by the condition number approach is clearly seen.

The high-frequency poles of truncated modal models are well known to be unreliable quantities; the high-frequency zeros of collocated structures have comparable sensitivity [8] and convergence [5] properties. The conclusion to be drawn from the present work is that the high-frequency zeros of non-collocated structures are even less robust. Care should therefore be taken when using the

zeros for, for instance, sensor/actuator placement [32][33] to consider only the low-frequency converged zeros in the analysis. It should be emphasized that the low-frequency zeros **are** reliable quantities, even in the non-collocated case; their convergence does not possess the Rayleigh-Ritz guarantee of monotonicity present for collocated structures, but is nonetheless rapid.

An interesting question which now arises is: for what values of p, as a function of n, do complex zeros arise? Table 4.1 summarizes the answer to this question: complex zeros exist for p values below p_1, real and imaginary zero pairs exist for p between p_1 and p_2; and purely imaginary zeros exist for p above p_2. It can be seen that the near-collocated case always yields only imaginary zeros, with the degree of non-collocation permissible decreasing as n increases. This makes sense. Real zeros appear for somewhat greater amounts of non-collocation, while even greater sensor/ actuator separation leads to the complex zero quadruples. It may initially appear to be paradoxical that the range of p values which gives complex zeros increases as n increases. We are, after all, approaching the distributed case, which never has complex zeros. However, the explanation is that it is only the unconverged high-frequency zeros which are actually complex. The effect of increasing model order is to give rise to more complicated, broader-ranging behavior for these zeros (compare Fig. 4.2 with Fig. 4.1), so leading to complex zeros for a wider range of p values. The lower-frequency zeros of these models do indeed converge to the purely real or imaginary "true" zeros as n increases, exactly as is to be expected. There is therefore no contradiction.

These transmission zero sensitivity results have obvious implications for the closed-loop performance that will be achievable as a function of actuator location. It should be expected that placing an actuator at a location which yields ill-conditioned zeros will lead to some sort of sensitivity in the closed-loop system. This is indeed the case, as can be seen graphically in Fig. 4.7. This plot shows the family of root loci that occur when output feedback is applied to a 6-mode model of the beam and the actuator position is varied from $p = 0.20$ to $p = 0.21$. As shown in Fig. 4.3, this range is one of extreme zeros sensitivity, with both the complex zero and the one

on the real axis changing considerably for very small actuator shifts. This leads to an interesting *switching* phenomenon in the root locus, whereby the root locus abruptly alters its configuration for an infinitesimal movement of the actuator. In particular, for low p the closed-loop pole that starts from the upper right of the figure asymptotically approaches the complex zero as the gain is increased; the smaller pole approaches the zero on the negative real axis. However, as p increases, the complex zero descends. Eventually, for an actuator normalized position of about 0.2038, the root locus branch from the lower pole becomes attracted to this zero, and the upper branch asymptotically approaches the real zero, which now has a magnitude of about 9. The extreme sensitivity of the zeros for this structural configuration is therefore directly reflected in severe sensitivity of the loci of the corresponding closed-loop poles.

For high gain, (3.15) predicts that the conditioning of a closed-loop pole will be approximately equal to that of the zero that it is asymptotically approaching. In particular, the closed-loop pole corresponding to the sensitive complex zero in Fig. 4.7 should itself have a high condition number when large gains are applied. Figs. 4.8 and 4.9 illustrate that this is indeed the case. The very close correspondence between the behavior of the condition number of the closed-loop pole (Fig. 4.8) and that of the zero (Fig. 4.9) can clearly be seen. (The difference in magnitudes between the two plots is merely a reflection of the details of the algorithms used to compute the two quantities, namely Wilkinson's method [12][13] for the pole and the generalized eigenvalue method of [11] for the zero; it is not significant.)

For the case of state feedback, the relationship between the sensitivity of the zeros and that of the closed-loop poles is not so direct. However, here too there appear to be connections between the zeros sensitivity profile shown previously and the condition numbers of the closed-loop poles. To illustrate this, the next two figures show the mean condition number of the closed-loop poles obtained for n = 6 if these poles are shifted to all have real parts of -0.5 (Fig. 4.10, the low gain case) or -2.0 (Fig. 4.11, high gain); the imaginary parts are all kept equal to those of the

corresponding open-loop poles. It can be seen that these plots exhibit the same type of localized extreme sensitivity as was shown in the zeros sensitivity profiles. A subject for further work is to examine why certain of the peaks coincide for both pole and zero plots while others appear to be shifted by the application of state feedback. A full understanding of this question is likely to provide a considerable degree of insight into practical state feedback control of flexible structures.

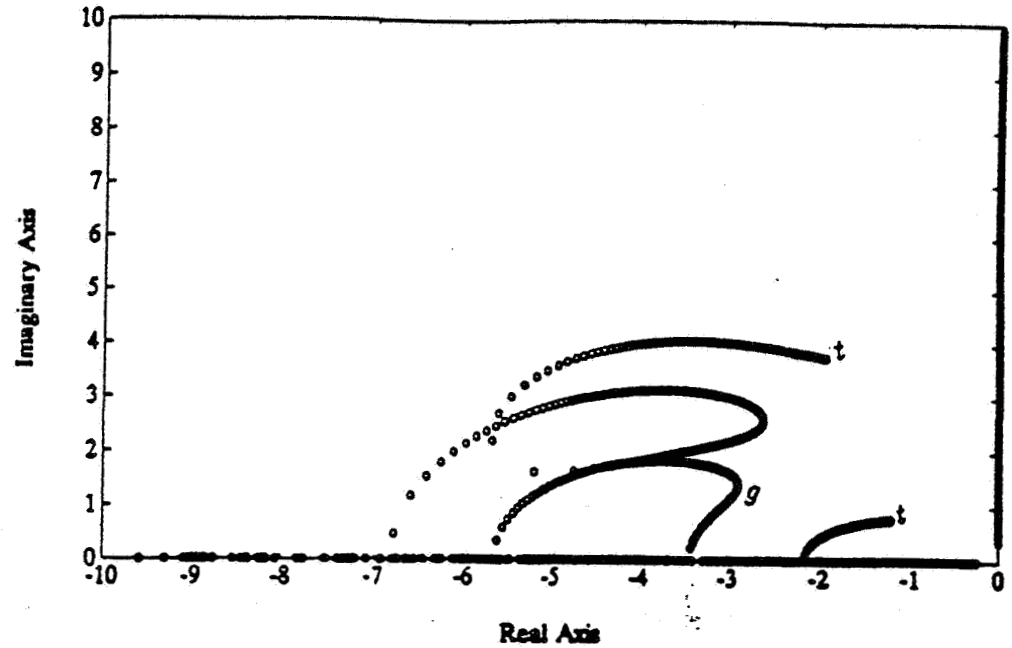

Figure 4.1. Zero locus for 6-mode beam model.

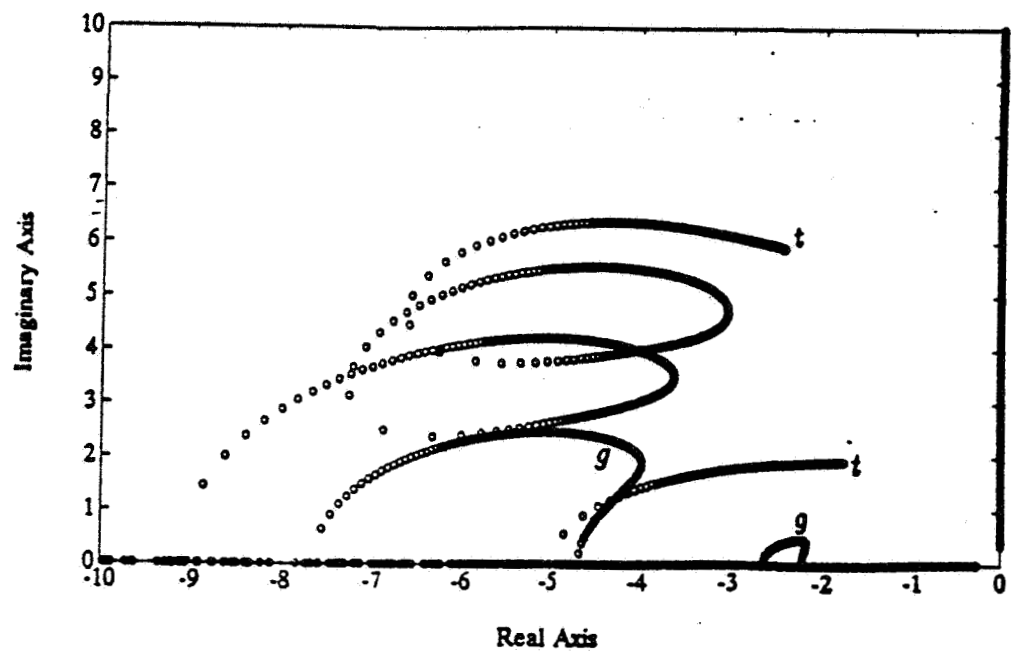

Figure 4.2. Zero locus for 7-mode beam model.

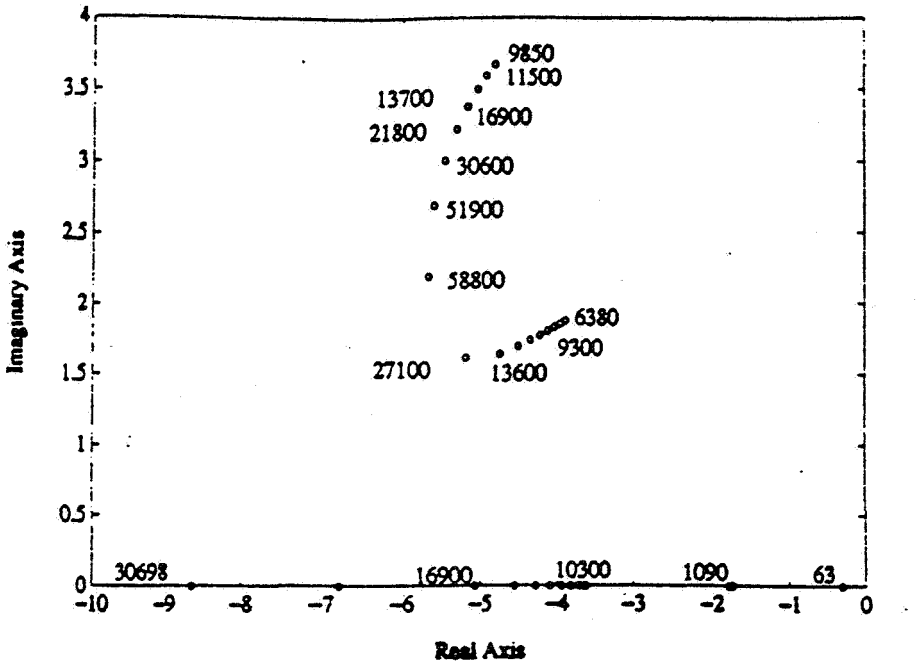

Figure 4.3. Zero locus for 6-mode beam model, 0.20 < p < 0.21.

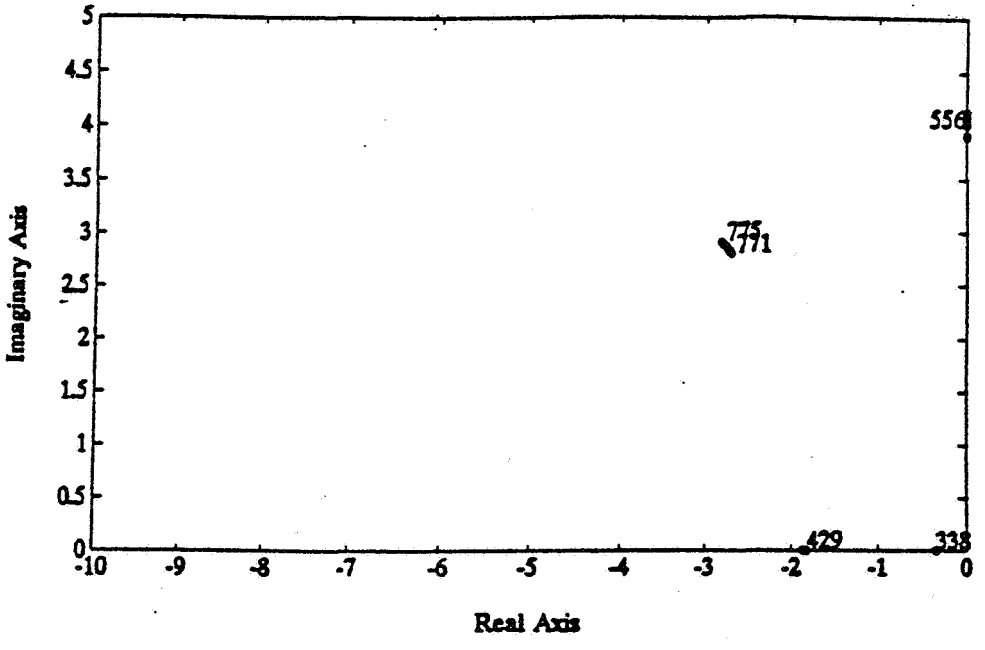

Figure 4.4. Zero locus for 6-mode beam model, 0.30 < p < 0.31.

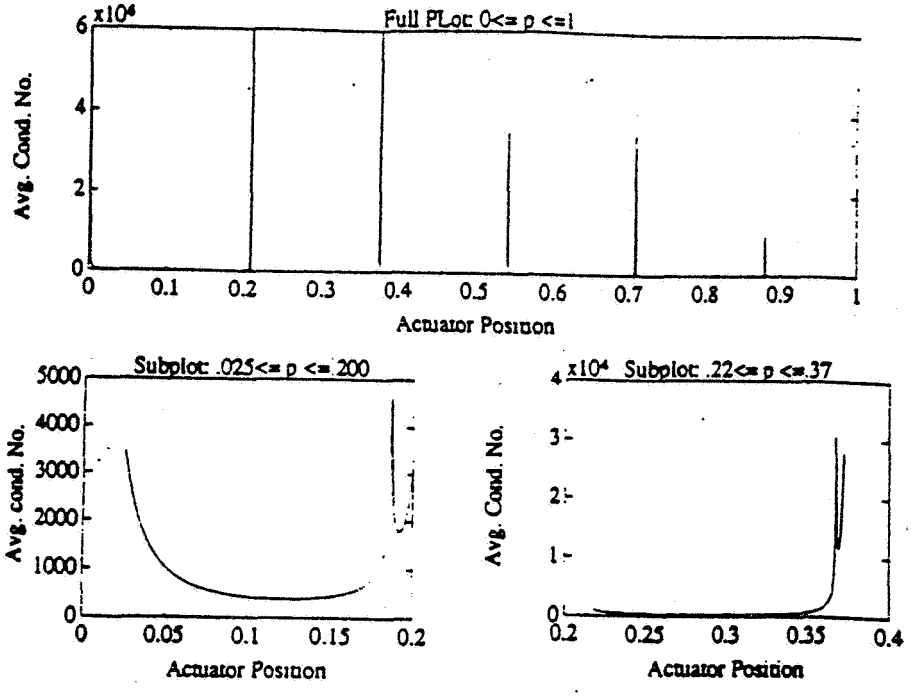

Figure 4.5. Zeros sensitivity profile for 6-mode beam model.

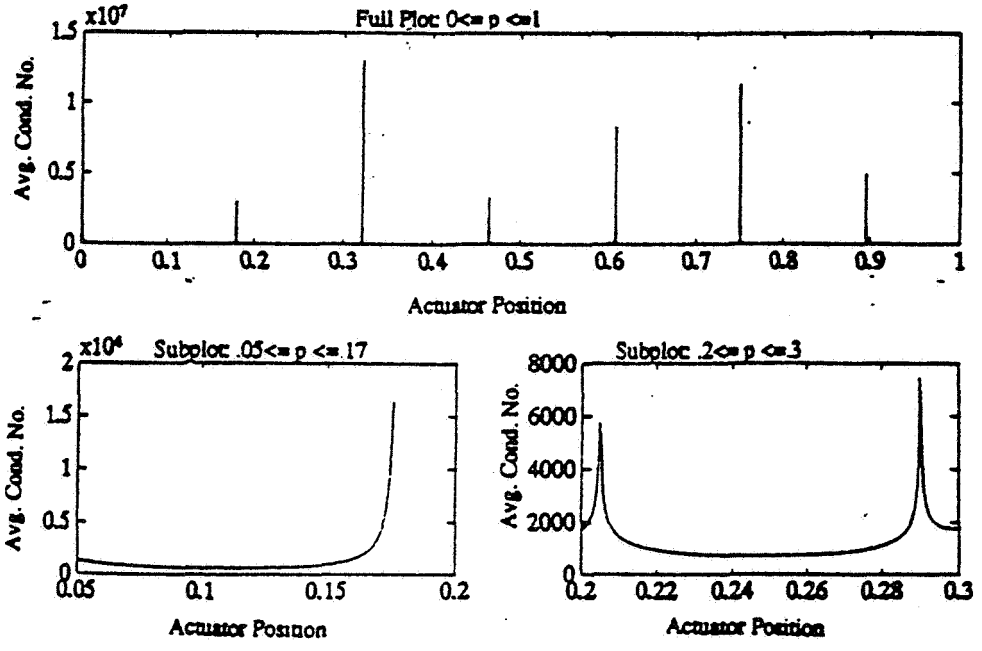

Figure 4.6. Zeros sensitivity profile for 7-mode beam model.

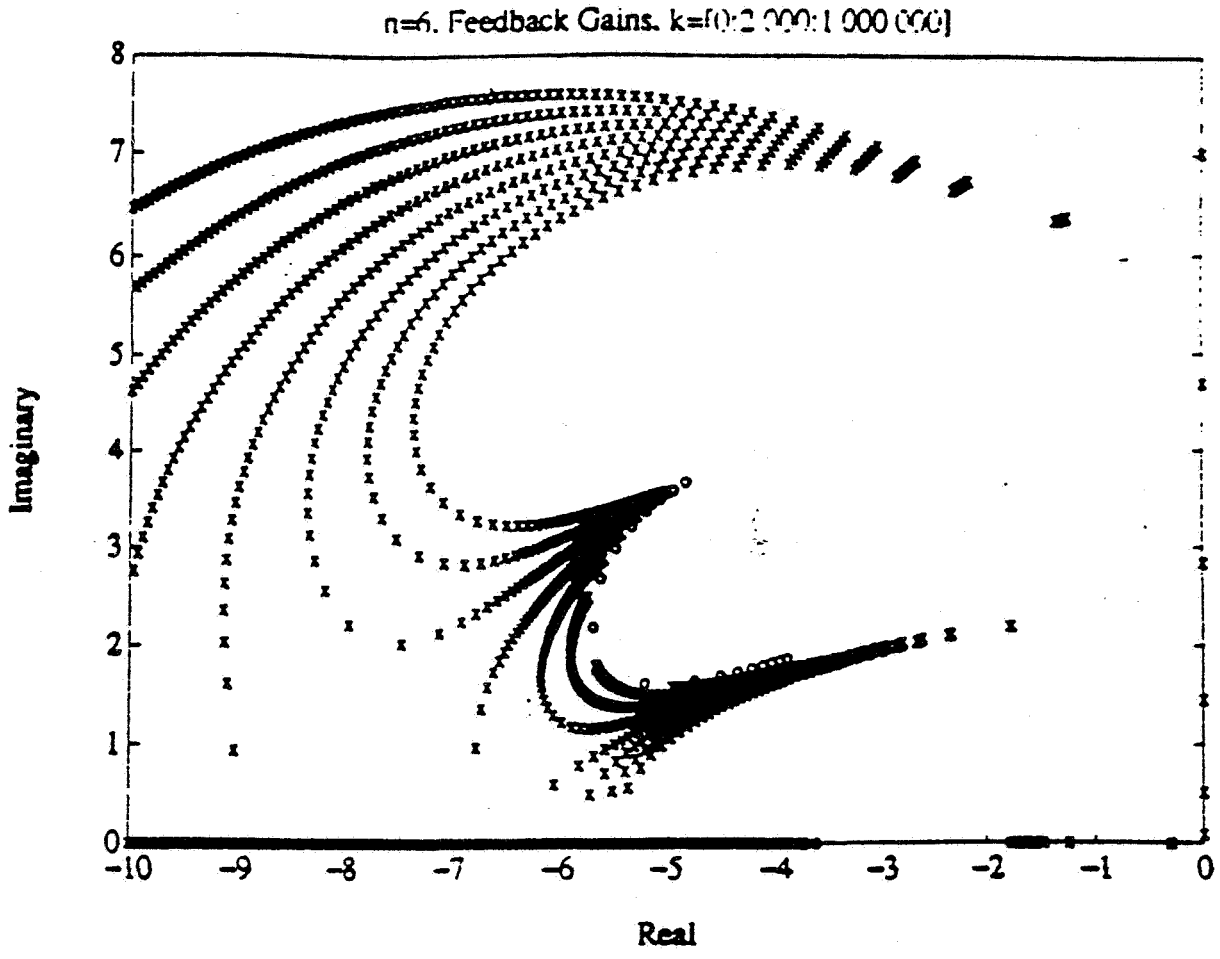

Figure 4.7. Root locus "switching" for sensitive zero location.

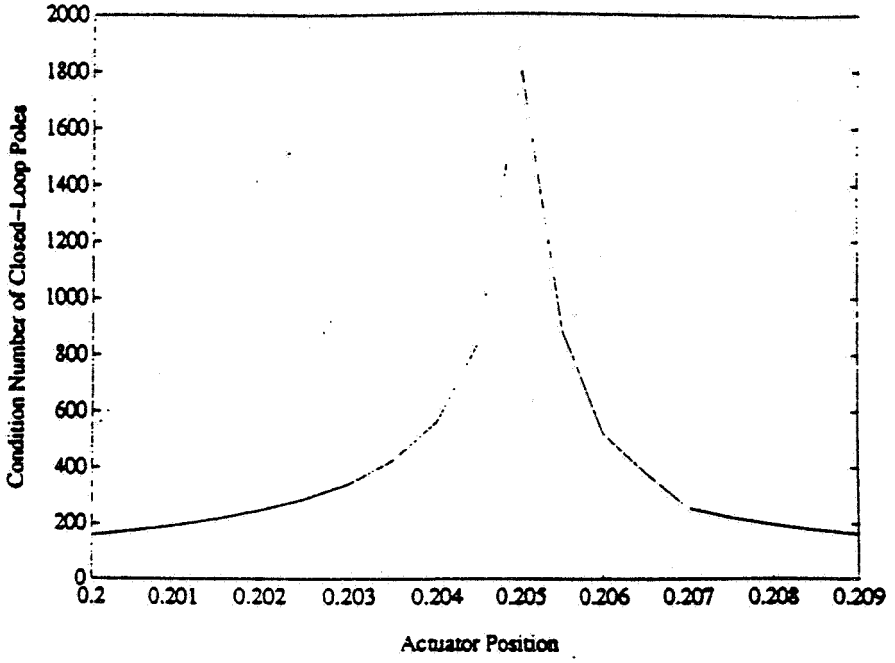

Figure 4.8. Condition number of closed-loop pole versus p.

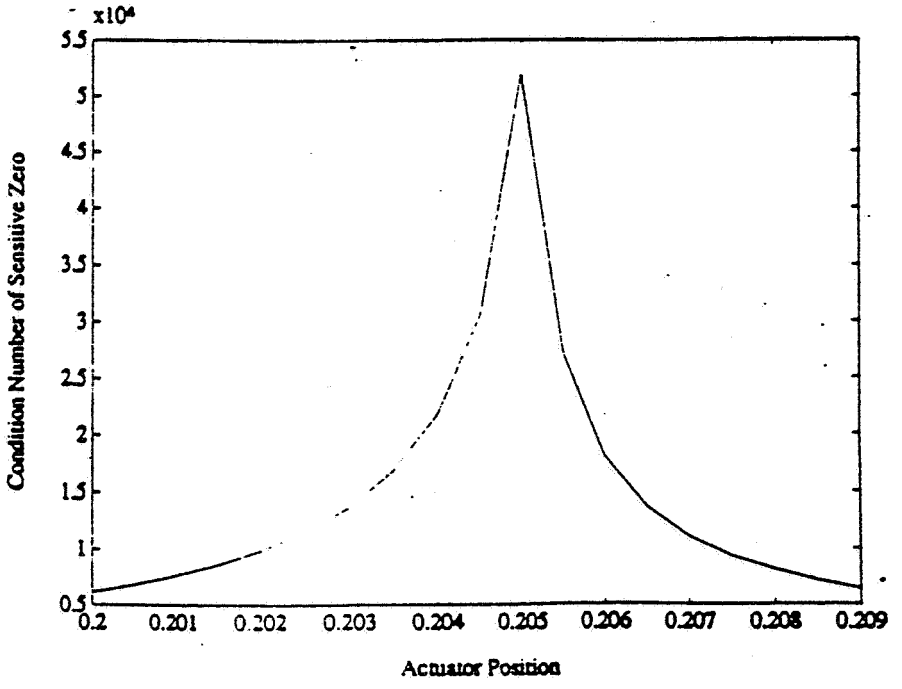

Figure 4.9. Condition number of zero versus p.

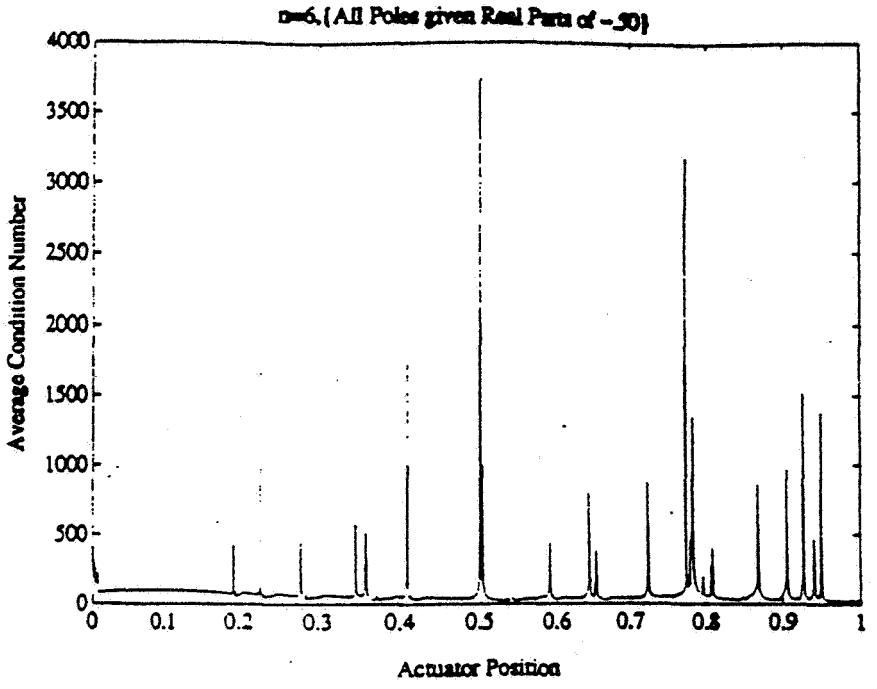

Figure 4.10. Closed-loop poles mean condition number, low gain.

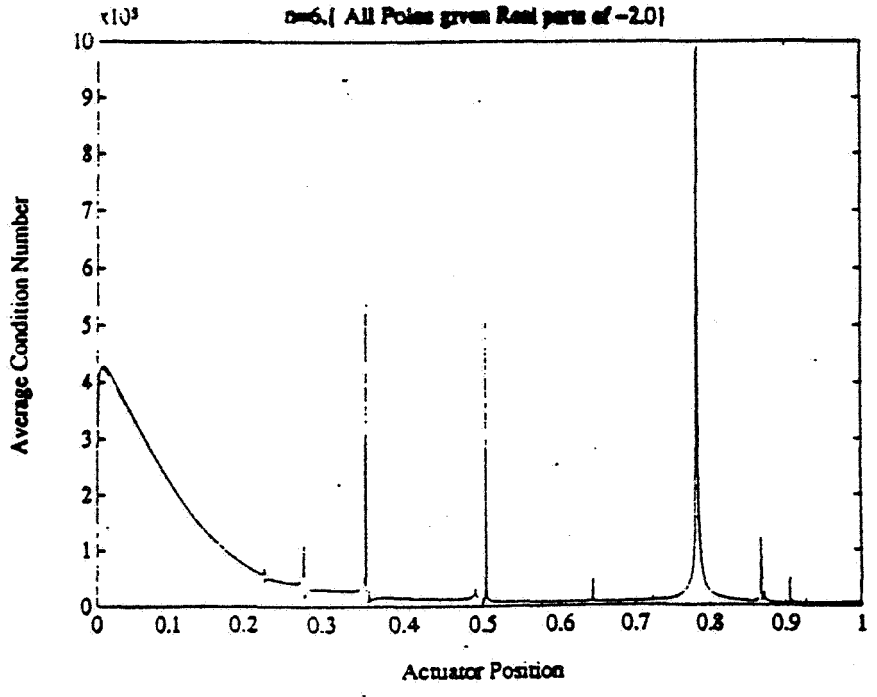

Figure 4.11. Closed-loop poles mean condition number, high gain.

5. Non-Interacting Instrument Placement

The problem to be studied in this portion of the report is that of selecting non-interacting locations at which to place a set of instruments on a given flexible structure. Such instruments are typically slewing telescopes, etc., and so can be regarded as pairs of collocated sensors and actuators; for simplicity in what follows, the measured outputs (e.g. instrument pointing angles) will be taken to be rates. (The structure may also possess other disturbance sources acting at different locations; this will be addressed later in the report.) The FSS is therefore of the form given by (2.1), with $\Phi_r = \Phi_a$ and $\Phi_d = 0$. The design problem is thus to select the matrix Φ_a so as to minimize the effects of the motion of each instrument on the measurements taken by the others. To do this, it will be necessary to first study the properties of the controllability and observability Grammians of flexible structures.

The controllability and observability Grammians, denoted by W_C and W_O, respectively, of this FSS are best described in terms of the state-space model corresponding to the state vector $\mathbf{x} = \begin{pmatrix} \dot{\eta}_1 & \omega_1\eta_1 & \cdots & \dot{\eta}_n & \omega_n\eta_n \end{pmatrix}^T$ For full generality, we shall study the property of these matrix quantities for an FSS with either displacement, rate or acceleration sensors. The resulting model $\{A, B, C, D\}$ is then of the form $A = blkdiag(A_i)$ and $B = \begin{pmatrix} B_1^T & \cdots & B_n^T \end{pmatrix}^T$, where

$$A_i = \begin{pmatrix} -2\zeta_i\omega_i & -\omega_i \\ \omega_i & 0 \end{pmatrix} \text{ and } B_i = \begin{pmatrix} \mathbf{b}_i \\ 0 \end{pmatrix}; \tag{5.1a}$$

$\mathbf{b}_i$ is the i^{th} row of Φ_a^T. The structure of the output equation $\mathbf{y} = C\mathbf{x} + D\mathbf{u}$ depends on whether displacement, rate or acceleration outputs are considered. Of the three cases, the most complicated is that of acceleration measurements, as accelerations are not state variables of the system. However, equation (1[a]) can be used to put this type of output into standard state form, giving $C_a\ddot{\boldsymbol{\eta}} = -C_a diag(2\zeta_i\omega_i)\dot{\boldsymbol{\eta}} - C_a diag(\omega_i^2)\boldsymbol{\eta} + C_a\hat{\mathbf{B}}\mathbf{u}$. The matrices $C = (C_1, \cdots, C_n)$ and D that describe the output equation are then given as follows for the three possible cases.

Displacement outputs: $C_i = \begin{pmatrix} 0 & \mathbf{c}_{d_i}/\omega_i \end{pmatrix}$, $D = 0$; (5.1b)

Rate outputs: $C_i = \begin{pmatrix} \mathbf{c}_{r_i} & 0 \end{pmatrix}$, $D = 0$; (5.1c)

Acceleration outputs: $C_i = \begin{pmatrix} -2\zeta_i\omega_i\mathbf{c}_{a_i} & -\omega_i\mathbf{c}_{a_i} \end{pmatrix}$, $D = C_a\hat{B}$; (5.1d)

$\mathbf{c}_{a_i}$, $\mathbf{c}_{r_i}$ and $\mathbf{c}_{d_i}$ are the i^{th} columns of C_a, C_r and C_d, respectively.

The Grammians are then given as the solutions of the algebraic Lyapunov equations

$$AW_c + W_c A^T + BB^T = 0 \tag{5.2}$$

and

$$A^T W_o + W_o A + C^T C = 0. \tag{5.3}$$

The block diagonal form of A can be exploited [16][18][19] to give closed-form solutions for these equations. These will now be discussed, first for the comparatively straightforward controllability case, and then for the more involved observability Grammian.

5.1 Closed-Form Controllability Grammian

Taking W_C first and writing it in terms of its (2 x 2) blocks $\{W_{ij}\}$, we have

$$A_i W_{ij} + W_{ij} A_j^T + B_i B_j^T = 0. \tag{5.4}$$

Applying (5.1) then yields, after some algebra, the expression

$$W_{ij} = \frac{\beta_{ij}}{d_{ij}} \cdot \begin{pmatrix} 2\omega_i\omega_j(\zeta_j\omega_i + \zeta_i\omega_j) & \omega_j(\omega_j^2 - \omega_i^2) \\ -\omega_i(\omega_j^2 - \omega_i^2) & 2\omega_i\omega_j(\zeta_i\omega_i + \zeta_j\omega_j) \end{pmatrix}, \tag{5.5}$$

where $\beta_{ij} = \mathbf{b}_i^T \mathbf{b}_j$ and $d_{ij} = 4\omega_i\omega_j(\zeta_i\omega_i + \zeta_j\omega_j)(\zeta_j\omega_i + \zeta_i\omega_j) + (\omega_j^2 - \omega_i^2)^2$. The quantity d_{ij}^{-1} is essentially a measure of how closely correlated modes i and j are; it will be returned to below. Evaluating W_C by this method involves about $7n^2$ floating-point operations (exploiting the symmetry of W_C, i.e. $W_{ji} = W_{ij}^T$); by contrast, the Bartels-Stewart algorithm [20] for general matrices A and B requires order(n^3) operations.

The general expression (5.5) for W_{ij} simplifies considerably for exactly repeated frequencies, where we obtain

$$W_{ij} = \frac{\beta_{ij}}{2(\zeta_i + \zeta_j)\omega_i} \cdot I_2; \tag{5.6}$$

in particular, the diagonal blocks are just $W_{ii} = \frac{\beta_{ii}}{4\zeta_i\omega_i} \cdot I_2$. Simplifications also occur for widely separated, lightly-damped modes: in this case,

$$W_{ij} \to \frac{\beta_{ij}}{(\omega_j^2 - \omega_i^2)} \cdot \begin{pmatrix} 0 & \omega_j \\ -\omega_i & 0 \end{pmatrix} \text{as } \zeta_i, \zeta_j \to 0. \tag{5.7}$$

It is important to note that (5.6) is inversely proportional to the damping ratios of the structure, while (5.7) is independent of damping. Thus, the only blocks of W_c which will be of significant magnitude for a structure with light damping are those on the diagonal, and those off-diagonal blocks that correspond to close frequencies. This reflects the well-known result [21]-[23] that the modal model of a flexible structure with widely separated natural frequencies is already approximately balanced. However, balancing a flexible structure with near-repeated frequencies is a much more challenging problem [16], as indeed is determining the controllability properties of its close modes [24].

5.2 Closed-Form Observability Grammian

The observability Grammian W_o is given as the solution of the algebraic Lyapunov equation (5.3). As was the case for W_c, closed-form expressions for the (2 x 2) blocks $\{W_{ij}\}$ making up W_o can be found by means of an equation analogous to (5.4). The details and complexity of the solutions obtained depend strongly on the structure of $C_i^T C_j$, which in turn is specified by the type of output considered. The expressions that result for the three possibilities (displacements, rates and accelerations) are as follows.

Displacement outputs:

The general expression in this case is

$$W_{ij} = \frac{\gamma_{ij}}{d_{ij}} \cdot \{2(\zeta_i\omega_i + \zeta_j\omega_j) \cdot \begin{pmatrix} 1 & 2\zeta_j \\ 2\zeta_i & 4\zeta_i\zeta_j \end{pmatrix} + \frac{1}{\omega_i\omega_j} \cdot \begin{pmatrix} 0 & -\omega_i(\omega_j^2 - \omega_i^2) \\ \omega_j(\omega_j^2 - \omega_i^2) & 2(\zeta_i\omega_i^3 + \zeta_j\omega_j^3) \end{pmatrix}\}, \tag{5.8}$$

where the scalar d_{ij} is as defined in (5.5), and $\gamma_{ij} = \mathbf{c}_{d_i}^T \mathbf{c}_{d_j}$. As was true for controllability, this simplifies considerably in certain special cases. In particular, for exactly repeated frequencies we have

$$W_{ij} = \frac{\gamma_{ij}}{2(\zeta_i + \zeta_j)\omega_i^3} \cdot \begin{pmatrix} 1 & 2\zeta_j \\ 2\zeta_i & 1+4\zeta_i\zeta_j \end{pmatrix}, \tag{5.9}$$

while for widely separated frequencies the expression becomes

$$W_{ij} \to \frac{\gamma_{ij}}{\omega_i\omega_j(\omega_j^2 - \omega_i^2)} \cdot \begin{pmatrix} 0 & -\omega_i \\ \omega_j & 0 \end{pmatrix} \text{as } \zeta_i, \zeta_j \to 0. \tag{5.10}$$

Consequently, the observability Grammian of a lightly damped structure with widely separated modes and displacement sensors will be diagonally dominant, with diagonal blocks $\{W_{ii} = \frac{\gamma_{ii}}{4\zeta_i\omega_i^3} \cdot \begin{pmatrix} 1 & 2\zeta_i \\ 2\zeta_i & 1+4\zeta_i^2 \end{pmatrix}\}$ approximately diagonal and inversely proportional to damping, and off-diagonal blocks damping-independent. As noted previously, however, this simple observation does not hold if the structure possesses repeated, or closely spaced, natural frequencies.

Rate outputs:

In this case, C^TC has the same form as the matrix BB^T; they are actually identical if sensors and actuators are colocated. Furthermore, it can be seen from (5.1) that A and its transpose are related by the expression $A^T = PAP$ with $P = diag\{1,-1,\ldots\}$, while $CP = C$ for rate measurements. Consequently, (5.3) can be rewritten as

$$A[PW_oP] + [PW_oP]A^T + C^TC = 0, \tag{5.11}$$

which is of the same form as the controllability Lyapunov equation (5.2). Thus, the observability Grammian for the case of rate measurements is essentially as given by (5.5), the only differences being that β_{ij} is replaced by $\gamma_{ij} = \mathbf{c}_{r_i}^T \mathbf{c}_{r_j}$ and the signs of the off-diagonal blocks are changed.

Acceleration outputs:

The general closed-form observability Grammian in this case is

$$W_{ij} = \frac{\gamma_{ij}\omega_i\omega_j}{d_{ij}} \cdot \{2\omega_i\omega_j(\zeta_j\omega_i + \zeta_i\omega_j) \cdot \begin{pmatrix} 4\zeta_i\zeta_j & 2\zeta_i \\ 2\zeta_j & 1 \end{pmatrix} + \begin{pmatrix} 2(\zeta_j\omega_i^3 + \zeta_i\omega_j^3) & -\omega_i(\omega_j^2 - \omega_i^2) \\ \omega_j(\omega_j^2 - \omega_i^2) & 0 \end{pmatrix}\}, \tag{5.12}$$

where $\gamma_{ij} = \mathbf{c}_{a_i}^T \mathbf{c}_{a_j}$. For exactly repeated frequencies, this simplifies considerably to

$$W_{ij} = \frac{\gamma_{ij}\omega_i}{2(\zeta_i + \zeta_j)} \cdot \begin{pmatrix} 1+4\zeta_i\zeta_j & 2\zeta_i \\ 2\zeta_j & 1 \end{pmatrix}, \tag{5.13}$$

and to

$$W_{ij} \to \frac{\gamma_{ij}\omega_i\omega_j}{(\omega_j^2 - \omega_i^2)} \cdot \begin{pmatrix} 0 & -\omega_i \\ \omega_j & 0 \end{pmatrix} \text{as } \zeta_i, \zeta_j \to 0 \tag{5.14}$$

for the case of widely separated frequencies. Consequently, W_o is diagonally dominant for a lightly damped structure with acceleration sensors if and only if it possesses no close modes. Quantifying the controllability and observability properties of structures when close modes *are* present will now be addressed in detail.

5.3 Closed-Form Cross-Grammian

If p ≥ m, as is typical of FSS applications, and there exists a matrix U with orthonormal columns which satisfies $C = UB^T P$, then the system is said to be *orthogonally symmetric* [25]. Flexible structures with collocated actuators and rate sensors form a particular class of orthogonally symmetric systems: as we then have $C = B^T$ and $B^T P = B^T$, we can simply take $U = I$. Associated with any orthogonally symmetric system is its *cross-Grammian* W_{co}, which is defined as the solution of the Lyapunov equation

$$AW_{co} + W_{co}A + BU^T C = 0. \tag{5.12}$$

The usefulness of W_{co} in balancing applications lies in the fact that it satisfies the relation $W_{co}^2 = W_c W_o$. In fact, as $C^T C = PBU^T UB^T P = BB^T$ and $BU^T C = BU^T UB^T P = BB^T$, (5.8) and (5.12) can be seen to reduce to the expressions [25]

$$W_{co} = W_c P = P W_o. \tag{5.13}$$

Thus, all three Grammians of an orthogonally symmetric system are given directly from (5.5) with suitable changes of sign, noting, of course, that $\beta_{ij} = \gamma_{rij}$ for such systems. This property will be shown to lead to significant simplifications when balancing models of collocated flexible structures.

6. Hankel Singular Values of Flexible Structures

It is always possible [26] to find a state transformation T that takes the model $\{A,B,C\}$ to an *internally balanced* state space representation $\{T^{-1}AT, T^{-1}B, CT\}$, i.e. one with equal and diagonal controllability and observability Grammians

$$\overline{W}_c = \overline{W}_o = \Sigma \equiv diag(\sigma_i), \tag{6.1}$$

where $\sigma_1 \geq \sigma_2 \geq \cdots \geq 0$. These *Hankel singular values (HSVs)* occur in approximately equal pairs for each flexible mode of a lightly-damped structure. Furthermore, they admit a very simple interpretation for any isolated mode: the corresponding HSVs are then just equal to the square root of the product of the *controllability* and *observability modal costs* [36] of this mode. The HSVs are more complicated, and provide a great deal of useful insight, in the practical case where the structure possesses modes with very close natural frequencies, for instance as a result of symmetry or repeated substructure elements. This case will be returned to in Sections 6.2 and 6.3 below, where the *degrees of controllability and observability* of close structural modes are analyzed. These variables quantify how certain of the balanced modes corresponding to a set of near-repeated physical modes can approach uncontrollability and/or unobservability as the frequency separation decreases to zero. An understanding of this phenomenon is a necessary underpinning to a complete analysis of the balanced model reduction procedure as it applies to a practical flexible structure with "clusters" of close natural frequencies.

6.1 Balanced Model Reduction

The Hankel singular values lead to a simple procedure for obtaining a reduced-order approximation to the original system: delete those balanced states corresponding to all singular values below some specified threshold. The resulting dominant reduced-order model will match the full system with an accuracy related to the sizes of those Hankel singular values which were discarded, so giving a guideline for selecting an acceptable reduced model order n_r; see [26] for further details. It should be noted that this model reduction procedure is very straightforward once the balancing

transformation T has been found: it merely amounts to discarding trailing rows of the balanced A and B and trailing columns of A and C.

Computation of T can be shown to amount to the solution of a standard eigenproblem. This can be formulated in various different ways: the one which follows is not the best numerically (see [26] for a superior alternative), but it makes the significance of the transformation T clearest. Inspection of (5.3) and (5.4) reveals that the Grammians of the balanced system are related to those of the original system model as

$$\overline{W}_c = T^{-1} W_c T^{-T} \text{ and } \overline{W}_o = T^T W_o T; \tag{6.2}$$

multiplying these matrices then gives

$$\Sigma^2 = \overline{W}_c \overline{W}_o = [T^{-1} W_c T^{-T}][T^T W_o T] = T^{-1}[W_c W_o]T. \tag{6.3}$$

Thus, T is just the matrix of eigenvectors (suitably scaled) of $W_c W_o$, and the Hankel singular values of the system are the corresponding eigenvalues. The usefulness of the cross-Grammian for balancing orthogonally symmetric systems can now also be seen: as T is the eigenvector matrix of $W_c W_o = W_{co}^2$ it is also the eigenvector matrix of W_{co}, and we have $T^{-1} W_{co} T = \Lambda$ with $\Sigma^2 = \Lambda^2$, so $\Lambda = diag(\pm\sigma_i)$. It can be shown [30] that the appropriate scaling for the eigenvectors making up T for a collocated flexible structure is such that the relation $T^T P T = P$ is satisfied, while the signs of the eigenvalues of W_{co} must alternate in the same way as the diagonal elements of P. This can certainly be seen to be true for the special case of light damping and widely spaced natural frequencies, as (5.13) and (5.7) then imply that the $\{\lambda_i\}$ occur in approximate pairs $\{\pm\beta_{ii}/4\zeta_i\omega_i\}$; similarly, the Hankel singular values $\{\sigma_i\}$ of a lightly-damped flexible structure always occur in approximate pairs. The important point about evaluating T in terms of the cross-Grammian directly, rather than using the product $W_c W_o$, is that it is a *square root* method. It therefore possesses the improved accuracy properties typical of these techniques, as exhibited by such applications as least squares estimation by QR decomposition rather than the normal equations [27], Kalman filtering [28], and the FSS problems of on-orbit structural identification [29] and transmission zeros computation [30].

6.2 Degrees of Controllability of Close Modes

Consider for simplicity a flexible structure with a pair of close modes at natural frequencies $\omega_i = \omega$ and $\omega_j = \omega(1+\varepsilon)$, $|\varepsilon| << 1$, with equal damping ratios $\zeta_i = \zeta_j = \zeta$. (Bounds similar to the expressions to be obtained below can be derived by means of Rayleigh quotients [13] for more than two close modes, but at the expense of additional complexity.)

The *degrees of controllability* of this pair of close modes will be defined to be the singular values of the corresponding (4 x 4) submatrix of W_c,

$$W = \frac{1}{4\zeta\omega} \cdot \begin{pmatrix} \overline{W}_{ii} & \overline{W}_{ij} \\ \overline{W}_{ij}^T & \overline{W}_{jj} \end{pmatrix}, \tag{6.4}$$

where, from (5.5) and (5.6),

$$\overline{W}_{ii} = \beta_{ii} \cdot I_2,\ \overline{W}_{jj} \approx \beta_{jj}(1-\varepsilon) \cdot I_2 \text{ and } \overline{W}_{ij} \approx \frac{\beta_{ij}\zeta}{(4\zeta^2+\varepsilon^2)} \cdot \begin{pmatrix} 2\zeta(2+\varepsilon) & \varepsilon(2+\varepsilon) \\ -\varepsilon(2-\varepsilon) & 2\zeta(2+\varepsilon) \end{pmatrix} \tag{6.5}$$

for $|\varepsilon| << 1$. These singular values, or *principal components* [14], provide a detailed measure of how controllable the highly-interacting modes i and j are. The analogous quantities for an isolated mode k are the two singular values of W_{kk}, or just the repeated values $\beta_{kk}/4\zeta_k\,\omega_k$, well-known [***3] as the *controllability modal cost* of this mode.

The matrix W is positive semi-definite symmetric, so [13] its singular values are precisely equal to its eigenvalues. These can in turn be shown [43] to be given as $\{\lambda = \mu/4\zeta\omega\}$, where $\{\mu\}$ are the four solutions of the characteristic equation

$$\det\left\{\mu^2 I_2 - \mu\left[\beta_{ii} + \beta_{jj}\right] I_2 + \left[\beta_{ii}\beta_{jj} \cdot I_2 - \overline{W}_{ij}^T \overline{W}_{ij}\right]\right\} = 0. \tag{6.6}$$

Furthermore, it can be shown that, for small ε,

$$\overline{W}_{ij}^T \overline{W}_{ij} \approx \frac{4\zeta^2\beta_{ij}^2}{(4\zeta^2+\varepsilon^2)} \cdot I_2 \equiv \alpha \cdot I_2. \tag{6.7}$$

This fact makes (6.6) particularly easy to solve, as the equation reduces approximately to the repeated scalar quadratic

$$\mu^2 - \mu\left[\beta_{ii} + \beta_{jj}\right] + \left[\beta_{ii}\beta_{jj} - \alpha\right] = 0. \tag{6.8}$$

This in turn implies that the degrees of controllability of modes i and j will occur in two near-repeated pairs of values. Each of these pairs corresponds to an uncorrelated internal mode (*principal vector* [14]) of the system, these modes being made up of linear combinations of the original physical vibration modes.

The degrees of controllability are particularly simple for the single input case. We then have that $\mathbf{b}_i$ and $\mathbf{b}_j$ are scalars, so $\beta_{ij}^2 = \beta_{ii}\beta_{jj}$ and the roots of (6.8) are just

$$\mu_{\max} = \tfrac{1}{2}(\beta_{ii} + \beta_{jj}) \cdot \left[1 + \sqrt{1-x}\right] \tag{6.9a}$$

and

$$\mu_{\min} = \tfrac{1}{2}(\beta_{ii} + \beta_{jj}) \cdot \left[1 - \sqrt{1-x}\right], \tag{6.9b}$$

where

$$x = \frac{4\beta_{ii}\beta_{jj}}{(\beta_{ii} + \beta_{jj})^2} \cdot \frac{\varepsilon^2}{(4\zeta^2 + \varepsilon^2)}. \tag{6.10}$$

(It is easy to show that x always lies in the interval [0, 1], so $\mu_{\max}$ and $\mu_{\min}$ are indeed real.) There is therefore, for small x, one internal mode which is strongly controllable and one which is weakly controllable, with the limiting case of exactly repeated frequencies producing an uncontrollable mode, as expected. Increasing the relative frequency separation ε obviously increases $\mu_{\min}$, while decreasing the damping ζ also increases it: this is even clearer for the special case of $|\varepsilon| << \zeta$, where we have $x \approx \dfrac{4\beta_{ii}\beta_{jj}}{(\beta_{ii} + \beta_{jj})^2} \cdot \dfrac{\varepsilon^2}{4\zeta^2} << 1$ and $\mu_{\min} \approx \tfrac{1}{4}(\beta_{ii} + \beta_{jj})x$. A physical interpretation for the role of damping in controllability can be given by considering the frequency response of a flexible structure. Decreasing the damping of two close modes reduces the widths of the corresponding amplitude peaks, so decreasing their overlap and increasing the extent to which one mode can be excited without exciting the other. This therefore increases controllability.

A final point should be noted. This is that no assumption of small ζ was made in the derivation of (6.9): thus, these results apply equally well to close modes of heavily-damped structures.

6.3 Degrees of Observability of Close Modes

A similar approach will now be taken in order to quantify the *degrees of observability* of two equally-damped close structural modes. As in the derivation of the closed-form observability Grammians previously, the three types of output measurements, described by (5.1[b]) - (5.1[d]), will be considered in turn. As will be seen, the results obtained for the three cases are very similar.

Displacement outputs:

The degrees of observability of the pair of close modes will be defined to be the singular values of the corresponding (4 x 4) submatrix of W_o,

$$W = \frac{1}{4\zeta\omega^3}\cdot\begin{pmatrix}\overline{W}_{ii} & \overline{W}_{ij}\\ \overline{W}_{ij}^T & \overline{W}_{jj}\end{pmatrix}. \tag{6.11}$$

Assuming $\omega_i = \omega$, $\omega_j = \omega(1+\varepsilon)$ and $\zeta_i = \zeta_j = \zeta$, the general expression (5.8) yields

$$\overline{W}_{ii} \approx \gamma_{ii}\cdot\begin{pmatrix}1 & 2\zeta\\ 2\zeta & 1\end{pmatrix},\ \overline{W}_{jj} \approx \gamma_{jj}(1-3\varepsilon)\cdot\begin{pmatrix}1 & 2\zeta\\ 2\zeta & 1\end{pmatrix} \tag{6.12}$$

and

$$\overline{W}_{ij} \approx \frac{2\gamma_{ij}\zeta}{(4\zeta^2+\varepsilon^2)}\cdot\begin{pmatrix}\zeta(2+\varepsilon) & -\varepsilon(1-\frac{1}{2}\varepsilon)+4\zeta^2\\ \varepsilon(1+\frac{1}{2}\varepsilon)+4\zeta^2 & \zeta(2+\varepsilon)\end{pmatrix}. \tag{6.13}$$

Note that the diagonal blocks $\overline{W}_{ii}$ and $\overline{W}_{jj}$ are only diagonally dominant for small damping ratios ζ. This differs from what was observed in the controllability problem, where these blocks were exactly scalar multiples of the (2 x 2) identity matrix. This difference complicates the following analysis somewhat; in particular, it implies that the degree of observability results that will now be obtained for displacement measurements are only valid for light damping.

The eigenvalues $\{\lambda\}$ of W can be written as $\lambda = \mu/4\zeta\omega^3$, where $\{\mu\}$ are given [43] from the characteristic equation

$$\det\begin{pmatrix}\mu I-\overline{W}_{ii} & -\overline{W}_{ij}\\ -\overline{W}_{ij}^T & \mu I-\overline{W}_{jj}\end{pmatrix} = \det\{\mu I-\overline{W}_{ii}\}\cdot\det\{(\mu I-\overline{W}_{jj})-\overline{W}_{ij}^T(\mu I-\overline{W}_{ii})^{-1}\overline{W}_{ij}\} = 0. \tag{6.14}$$

After some algebra, this expression can be shown to reduce, for the case of light damping, to the approximately repeated scalar quadratic equation (6.8), with $\{\beta_{ij}\}$ replaced by $\{\gamma_{ij}\}$ in both this

equation and (6.7). Thus, the remarks made previously concerning the role of damping ratio and frequency separation in the degrees of controllability of close modes apply equally well to observability with displacement sensors.

Rate outputs:

The duality already noted between observability with rate measurements and controllability implies that the degree of controllability results obtained above quantify equally well the degrees of observability for this case. The only modification required to equations (6.6) - (6.9) is that of replacing the scalars $\{\beta_{ij}\}$ by $\{\gamma_{ij}\}$. As was the case for the controllability analysis, these results are valid for all levels of damping.

Acceleration outputs:

The submatrix of W_o that must be studied in this case has the form

$$W = \frac{\omega}{4\zeta} \cdot \begin{pmatrix} \overline{W}_{ii} & \overline{W}_{ij} \\ \overline{W}_{ij}^T & \overline{W}_{jj} \end{pmatrix}, \tag{6.15}$$

where the individual blocks are given from (5.12) as

$$\overline{W}_{ii} \approx \gamma_{ii} \cdot \begin{pmatrix} 1 & 2\zeta \\ 2\zeta & 1 \end{pmatrix}, \; \overline{W}_{jj} \approx \gamma_{jj} \cdot \begin{pmatrix} 1+\varepsilon & 2\zeta \\ 2\zeta & 1+\varepsilon \end{pmatrix} \tag{6.16}$$

and

$$\overline{W}_{ij} \approx \frac{2\gamma_{ij}\zeta}{(4\zeta^2+\varepsilon^2)} \cdot \begin{pmatrix} \zeta(2+5\varepsilon) & -\varepsilon(1+\frac{3}{2}\varepsilon)+4\zeta^2 \\ \varepsilon(1+\frac{5}{2}\varepsilon)+4\zeta^2 & \zeta(2+5\varepsilon) \end{pmatrix}. \tag{6.17}$$

Just as was found for displacement measurements, these diagonal blocks are diagonal only to first order in ζ. Consequently, the degree of observability results obtained for this case will also only be valid for lightly damped modes.

The eigenvalues of W can be written as $\{\lambda = \mu \cdot \omega/4\zeta\}$, where $\{\mu\}$ are again given from a characteristic equation of the form (6.14). For light damping, this determinant can once again be shown to reduce to the approximately repeated scalar quadratic equation (6.8), with $\{\beta_{ij}\}$ replaced

by $\{\gamma_{ij}\}$ throughout. Thus, the roles of damping ratio and frequency separation in the degrees of controllability of close modes carry over unchanged to observability with acceleration sensors. It can therefore be seen that the only significant difference between the degrees of observability obtained for the three possible types of sensors lies in the frequency dependence of the scale factor $1/4\zeta\omega^3$ (displacements), $1/4\zeta\omega$ (rates) or $\omega/4\zeta$ (accelerations) that must be applied to them.

7. Optimal Instrument Perturbations

The background provided above allows us to derive two computationally efficient techniques for deciding how to move the instruments so as to minimize their disturbance interactions. In both cases, the basic procedure is the same: each instrument in turn is moved through some small displacement, in a direction chosen so as to reduce the observability of the overall system as much as possible. This procedure is repeated until convergence to an acceptable set of instrument locations is obtained. Note that the procedures will be shown to be applicable equally well to discrete structures (e.g. trusses) or continuous ones (e.g. plates and beams). The implementational details of course differ for the two types of structure, as will be discussed in Section 8.

The two approaches to be described differ only in the definition of the observability measure that is to be minimized. In the first case, this is the largest Hankel singular value of the structure, while in the second it is the sum of the Hankel singular values. This choice in turn alters the expression for the optimal direction in which each instrument is to be moved at each step. The two methods will now both be described in turn.

7.1 Minimizing Largest Hankel Singular Value

Consider the case of shifting the k^{th} instrument on the structure, all other instruments remaining fixed for now. This alters only column k of the influence matrix Φ_a^T, i.e. the k^{th} entries of each of the row vectors $\mathbf{b}_i$ in (5.1) etc. The change in this column can be used to reduce the largest Hankel singular value of the system as much as possible by examining the resulting first-order perturbation of this quantity. As the system considered is orthogonally symmetric, its Hankel singular values are just the eigenvalues of the cross-Grammian W_{co}. Thus, the eigenvalue perturbation results of Stewart [13] can be applied directly to this problem.

Let λ be the largest Hankel singular value of the system, i.e. the largest eigenvalue of the cross-Grammian. It therefore satisfies the left and right eigenequations

$$W_{co}\mathbf{x} = \lambda\mathbf{x} \tag{7.1}$$

and

$$\mathbf{y}^H W_{co} = \lambda\mathbf{y}^H, \tag{7.2}$$

where it should be noted that the matrix W_{co} is not in general symmetric (see (5.13)). If $\mathbf{x}$ and $\mathbf{y}$ are normalized so as to satisfy $\|\mathbf{x}\|_2 = 1$ and $\|\mathbf{y}\|_2 = 1$, then the change in this eigenvalue in response to a change δW_{co} in the cross-Grammian is, to first order,

$$\delta\lambda \approx \frac{1}{|\mathbf{y}^H\mathbf{x}|} \cdot \mathbf{y}^H \delta W_{co}\mathbf{x}. \tag{7.3}$$

This eigenvalue perturbation result is general; however, the specifics of the problem considered here can now be exploited to simplify it. The two points to be made are as follows:

Symmetric formulation for $\mathbf{y}^H \delta W_{co}\mathbf{x}$.

Combining equations (5.13) and (7.2), we have that

$$\mathbf{y}^H W_c P = \lambda\mathbf{y}^H. \tag{7.4}$$

Now, the controllability Grammian W_c is symmetric, so this can be transposed to give

$$PW_c\mathbf{y} = \lambda\mathbf{y}, \tag{7.5}$$

which implies, as $PP = I$, that $PW_cPP\mathbf{y} = \lambda\mathbf{y}$. After pre-multiplying by P this yields

$$W_{co}[P\mathbf{y}] = \lambda[P\mathbf{y}]. \tag{7.6}$$

Comparing this with (7.1) and noting that $\mathbf{x}$ and $\mathbf{y}$ are both normalized, we clearly have that

$$\mathbf{x} = P\mathbf{y}, \tag{7.7}$$

so the desired symmetric expression is simply

$$\begin{aligned} \mathbf{y}^H \delta W_{co}\mathbf{x} &= \mathbf{y}^H \delta W_{co} P\mathbf{y} \\ &= \mathbf{y}^H \delta W_c \mathbf{y}, \end{aligned} \tag{7.8}$$

where δW_c is the perturbation of the symmetric controllability Grammian resulting from the shift in instrument location. It should be borne in mind, of course, that $\mathbf{y}$ is a left eigenvector of the unsymmetric cross-Grammian W_{co}, not of W_c.

Closed-form δW_c:

As already noted, shifting the k[th] instrument location alters only column k of the matrix Φ_a^T. The resulting effect on the controllability Grammian is thus to alter the scalars β_{ij} in the closed-form expressions (5.5); all other quantities remain unchanged. In detail, the change in the (2 x 2) (i,j)[th] block of W_c can be written as

$$\delta W_{ij} = \delta\beta_{ij} \cdot \hat{W}_{ij}, \tag{7.9}$$

where $\hat{W}_{ij} \equiv W_{ij} / \beta_{ij}$, with notation as in (5.5). Furthermore,

$$\delta\beta_{ij} = \{\mathbf{b}_i + (0 \quad \cdots \quad \delta b_{ik} \quad \cdots \quad 0)\}\{\mathbf{b}_j^T + \begin{pmatrix} 0 \\ \vdots \\ \delta b_{jk} \\ \vdots \\ 0 \end{pmatrix}\} - \mathbf{b}_i\mathbf{b}_j^T \tag{7.10}$$

$$\approx \delta b_{ik} \cdot b_{jk} + \delta b_{jk} \cdot b_{ik},$$

neglecting second-order terms.

Combining equations (7.8) and (7.10), the eigenvalue perturbation expression (7.3) can finally be rewritten as

$$\delta\lambda \approx \frac{1}{|\mathbf{y}^H P \mathbf{y}|} \cdot \mathbf{y}^H \delta W_c \mathbf{y}. \tag{7.11}$$

The positive scalar multiplier $1/|\mathbf{y}^H P\mathbf{y}|$ is not important when trying to find optimal instrument shift directions, and so will be omitted here. The remaining term can be expanded as

$$\begin{aligned} \mathbf{y}^H \delta W_c \mathbf{y} &= \sum_i \sum_j \mathbf{y}_i^H \delta W_{ij} \mathbf{y}_j \\ &= \sum_i \sum_j \delta\beta_{ij} \cdot \mathbf{y}_i^H \hat{W}_{ij} \mathbf{y}_j, \end{aligned} \tag{7.12}$$

where the 2-vectors $\{\mathbf{y}_i\}$ are defined as

$$\mathbf{y} = \begin{pmatrix} \mathbf{y}_1 \\ \vdots \\ \mathbf{y}_n \end{pmatrix}. \tag{7.13}$$

Defining the constant scalars $\{\alpha_{ij}\}$ to be

$$\alpha_{ij} = \mathbf{y}_i^H \hat{W}_{ij} \mathbf{y}_j, \tag{7.14}$$

we can therefore write (7.12) as

$$\begin{aligned} \mathbf{y}^H \delta W_c \mathbf{y} &= \sum_i \sum_j \delta\beta_{ij} \cdot \alpha_{ij} \\ &= \sum_i \sum_j \alpha_{ij} (\delta b_{ik} \cdot b_{jk} + b_{ik} \cdot \delta b_{jk}), \end{aligned} \tag{7.15}$$

making use of (7.10). Defining the matrix $\tilde{A} = (\alpha_{ij})$, this can be expressed in the simple vector-matrix form

$$\begin{aligned} \mathbf{y}^H \delta W_c \mathbf{y} &= \begin{pmatrix} b_{1k} & \cdots & b_{nk} \end{pmatrix} [\tilde{A} + \tilde{A}^T] \begin{pmatrix} \delta b_{1k} \\ \vdots \\ \delta b_{nk} \end{pmatrix} \\ &= \mathbf{b}_{col\_k}^T [\tilde{A} + \tilde{A}^T] \delta \mathbf{b}_{col\_k}, \end{aligned} \tag{7.16}$$

where $\mathbf{b}_{col\_k}$ is the kth column of Φ_a^T. Now, the design problem is to shift instrument k so as to reduce the maximal Hankel singular value λ as much as possible. The last equation allows us to achieve this, as the quantity

$$\mathbf{p}^T = \mathbf{b}_{col\_k}^T [\tilde{A} + \tilde{A}^T] \tag{7.17}$$

is a vector which is entirely in terms of known quantities. Thus, if the instrument perturbation is chosen to be as nearly as possible anti-parallel to this known vector, i.e. of the form

$$\delta \mathbf{b}_{col\_k} = -\mu \mathbf{p} \tag{7.18}$$

for some positive scalar μ, then the resulting eigenvalue perturbation will be as large and negative as possible for all instrument perturbations of this magnitude. Thus, λ will be reduced by the maximum amount possible.

7.2 Minimizing Sum of Hankel Singular Values

In this case, the observability measure to be minimized is not the largest Hankel singular value of the system, but rather the sum of the Hankel singular values. This quantity is just the trace of the controllability Grammian W_c; by the closed-form expression (5.7) it can be written as

$$trace(W_c) = \sum_i \frac{\beta_{ii}}{2\zeta_i\omega_i}. \tag{7.19}$$

Again, shifting instruments only affects the scalars $\{\beta_{ij}\}$, altering them to first-order by perturbations given by (7.10). Here, we are only concerned with the diagonal terms $\{\beta_{ii}\}$; a shift of the k^{th} instrument causes changes of the form

$$\delta\beta_{ii} \approx 2\delta b_{ik} \cdot b_{ik} \tag{7.20}$$

in these. The resulting change in the trace of W_c is therefore

$$\begin{aligned} \delta trace(W_c) &= \sum_i \frac{\delta\beta_{ii}}{2\zeta_i\omega_i} \\ &\approx \sum_i \frac{\delta b_{ik} \cdot b_{ik}}{\zeta_i\omega_i}, \end{aligned} \tag{7.21}$$

which can be written in inner-product form as

$$\delta trace(W_c) \approx \mathbf{q}^T \delta\mathbf{b}_{col\_k}, \tag{7.22}$$

where

$$\mathbf{q} = \begin{pmatrix} b_{1k} / (\zeta_1\omega_1) \\ \vdots \\ b_{nk} / (\zeta_n\omega_n) \end{pmatrix} \tag{7.23}$$

and $\delta\mathbf{b}_{col\_k}$ is as before. Now, the vector $\mathbf{q}$ is given purely in terms of known quantities, as was the vector $\mathbf{p}$ in the previous analysis. Furthermore, it plays a very similar role to that vector; if the k^{th} instrument shift is chosen as nearly as possible anti-parallel to $\mathbf{q}$, i.e. satisfying

$$\delta\mathbf{b}_{col\_k} = -\mu\mathbf{q} \tag{7.24}$$

for some positive scalar μ, then this will reduce the sum of the Hankel singular values of the system as much as possible. The differences between the two methods discussed therefore lie only in the details of the construction of the vector used to determine the optimum instrument shift direction. The vector $\mathbf{q}$ is certainly simpler and faster to compute than is $\mathbf{p}$, as it does not involve finding an eigenvector of W_{co}. In addition, the two methods often produce very similar results in practice. However, it has also been observed that the algorithm based on $\mathbf{q}$ can, on occasion, converge to an undesirable local minimum; details will be given in the next section. It therefore

appears advisable in practice to carry out the additional calculations required for the **p** method, in order to avoid possible convergence problems.

8. Implementational Details

Various practical details should be borne in mind when implementing the two instrument placement methods just derived. If sufficient care is taken with these points, the efficiency of the resulting algorithms, together with their convergence properties and generality of application, can be improved considerably.

Considering computational efficiency first, there are several ways in which the operation counts required for the maximal Hankel singular value technique can be minimized. (The method based on the sum of the HSVs is already extremely efficient, and cannot really be improved further.) The main point to note is that we only need the eigenvector $\mathbf{y}$ corresponding to the maximal eigenvalue, λ, of W_{co}. It is therefore certainly not necessary to evaluate the entire eigenstructure of the cross-Grammian, only to discard the bulk of it. Instead, a method closely related to the *power method* [12] can be used to iteratively compute $\mathbf{y}$ and λ, at very low computational cost. The standard power method cannot be used itself, as it requires that the maximal eigenvalue be considerably greater than the next largest. However, W_{co} always has two approximately equal maximal eigenvalues, $\pm|\lambda|$, for a lightly-damped structure; thus, the power method would not converge. Instead, the *orthogonal iteration* [27] technique can be used to iteratively find these two eigenvalues and their associated eigenvectors. The procedure starts by selecting a (2n x 2) matrix Q_0 as an initial approximation to a basis for the desired eigenspace. The iteration then proceeds to generate a sequence of matrices $\{Q_i\}$ as follows:

$$
\begin{aligned}
&i = 1,2,\cdots: \\
&Z_i^T = Q_{i-1}^T W_{co}; \\
&Q_i R_i = Z_i,
\end{aligned}
\tag{8.1}
$$

the *QR decomposition* [27] of Z_i. Convergence of the $\{Q_i\}$ to the required eigenspace is generally rapid if Q_0 is chosen suitably. Fortunately, in the present application there are two points which make this choice rather straightforward. Firstly, the special structure of W_{co} for a lightly-damped flexible structure allows Q_0 to be determined by inspection whenever the natural frequencies are widely spaced. Secondly, when cycling through the instrument placement algorithm, the

converged Q_i from the previous cycle will generally be a very good choice for Q_0 for the current one. In fact, it may be possible to use the previous eigenmatrix directly, with no manipulation, over several cycles and still obtain sufficient accuracy for our purposes.

Two points concerning the matrix $\tilde{A}$ can also be noted to speed up computation as much as possible. Firstly, if the vector **y** is real (as has been observed to be the case in practice for lightly-damped flexible structures, but has not been proven, as the cross-Grammian is not symmetric), then $\tilde{A}$ will always be symmetric. It is therefore not strictly necessary to introduce its transpose into (7.16) and (7.17). Secondly, if all instruments are to be moved at each cycle through the algorithm, it is only actually necessary to compute $\tilde{A}$ once per cycle; it can then be used unchanged to calculate the optimal directions of motion for each of the instruments simultaneously. In fact, (7.17) and (7.18) taken for all values of k together give the matrix equation

$$\delta B = -[\tilde{A} + \tilde{A}^T]\Phi_a^T M \tag{8.2}$$

for some positive diagonal matrix M. The optimal shift for instrument k is then such that the change in its influence vector is as nearly as possible parallel to column k of the matrix δB.

A further practical point that must be borne in mind when implementing either of the instrument placement algorithms is that the optimal $\delta \mathbf{b}_{col\_k}$ will not, in general, correspond to a physically realizable instrument shift. For instance, an instrument at an interior point on a plate can be moved in any desired direction in the *(x,y)* plane of the plate, but not out-of-plane. Let the vectors $\partial \mathbf{b}_{col\_k}/\partial x$ and $\partial \mathbf{b}_{col\_k}/\partial y$ denote the partial derivatives of the instrument influence vector for motion along the two in-plane axes, and define the matrix $X = \left(\partial \mathbf{b}_{col\_k}/\partial x \quad \partial \mathbf{b}_{col\_k}/\partial y\right)$. Then the physically realizable instrument shift that is closest to the desired optimal movement in a least squares sense is given by the orthogonal projection equation

$$\begin{pmatrix} \delta x \\ \delta y \end{pmatrix} = [X^T X]^{-1} X^T \delta \mathbf{b}_{col\_k}. \tag{8.3}$$

For a discrete truss-like structure, the only perturbation possible for an instrument which is currently positioned at a particular node is to shift it to one of the few adjacent nodes. However, it is still possible to use an equation analogous to (8.3) to determine which feasible shift is closest to the desired optimal $\delta \mathbf{b}_{col\_k}$ in a least squares sense. One practical detail here is as follows. It has been found in numerous simulation studies that superior results are obtained when the shift direction chosen is that which has the smallest angle to $\delta \mathbf{b}_{col\_k}$, rather than that which has the largest projected component along it. In other words, the magnitudes of the feasible instrument influence vector shifts should not be considered when selecting the direction in which to move.

In the placement algorithms developed so far, the only disturbances acting on each instrument were the motions resulting from the slewing of the other instruments. However, there may in practice be other disturbance sources present on the structure as well. Fortunately, the basic algorithms as derived above can be extended, at the cost of some additional complexity, to deal with this generalized problem.

In particular, consider a flexible structure with a set of disturbance sources at known positions on it. We wish to place a set of instruments on the structure so as to minimize the total effect of disturbances and instrument cross-coupling on the pointing accuracy of each instrument. The main additional complexity that now arises is the fact that the system is no longer collocated; thus, the cross-Grammian cannot be used to find the Hankel singular values. Instead, these values must be computed as the square roots of the eigenvalues of $W_c W_o$, where the Grammians W_c and W_o can still be obtained in closed-form as before.

In outline, the placement procedure based on the maximal HSV is now as follows; the method based on the sum of the HSVs can be generalized in analogous fashion. Let λ be the maximal Hankel singular value of the system. Its square then satisfies the left and right eigenequations

$$W_c W_o \mathbf{x} = \lambda^2 \mathbf{x} \tag{8.4}$$

and

$$\mathbf{y}^H W_c W_o = \mathbf{y}^H \lambda^2, \tag{8.5}$$

where $\mathbf{x}$ and $\mathbf{y}$ are assumed to be normalized. The effect of a small change in the product of the Grammians, for instance as a result of a small shift in an instrument position, is then to perturb this squared HSV to

$$\overline{\lambda}^2 \approx \lambda^2 + \mathbf{y}^H \delta(W_c W_o)\mathbf{x}, \tag{8.6}$$

by the standard first-order eigenvalue result. But we also have, to first order,

$$\delta(W_c W_o) \approx W_c \delta W_o + \delta W_c W_o. \tag{8.7}$$

Furthermore, if the perturbation in the Grammians is a result of shifting the k^{th} instrument, then the changes in these matrices will actually be a result of altering the scalar multipliers $\{\beta_{ij}\}$ and $\{\gamma_{rij}\} = \mathbf{c}_{ri}^T \mathbf{c}_{rj}$ etc. in the closed-form expressions (5.5) and (5.11). The changes in these quantities can be computed quite simply using equation (7.10). Thus, the perturbation in the maximal HSV that results from an instrument shift on a non-collocated structure can be readily computed.

Finally, both of the instrument placement techniques described above can easily be applied to structures with varying modal parameters. This is a consequence of the closed-form nature of the Hankel singular value expressions which form the basis of these algorithms. For, if the natural frequencies, damping ratios and/or mode shapes of the structure in question change as a result of alterations to its structural elements, these changes directly influence the closed-loop Grammians (5.5) and (5.11) and the influence matrix Φ_a^T. The changes in the optimal shift directions $\mathbf{p}$ and $\mathbf{q}$ that result from these changes are therefore easily characterized. The new instrument placement algorithms thus appear to be natural components of an integrated controls-structure design approach, where both control system parameters (e.g. positions of instruments) and structural parameters (e.g. stiffnesses of truss members) are varied in such a way as to maximize closed-loop performance while minimizing overall system mass. This type of approach is very promising when compared to the classical approach where structure and control system are designed in sequence.

9. Instrument Placement Results

The instrument placement algorithms derived and analyzed in the last four sections will now be illustrated by application to two flexible structures. The first, a uniform rectangular plate, is typical of structures modeled as continua, where instruments can be placed at any desired position. The second example, the Air Force Phillips Laboratory *A*dvanced *S*pace Structures *T*echnology *R*esearch *Ex*periment (ASTREX) testbed, is representative of truss-like discrete structures, where instruments can only be positioned at the node points. Each of these systems serves to illustrate different aspects of the HSV-based placement algorithms.

9.1 Uniform Plate Model

We shall now consider a uniform vertical steel plate model which is based on the DFVLR laboratory test article described in [37]. This plate has horizontal length 1.50 m, vertical length 2.75 m, thickness 2 mm, and isotropic material properties $E = 2.0 \times 10^{11}$ N/m^2, $\rho = 8.0 \times 10^3$ kg/m^3 and $\nu = 0.3$. In this study, a damping ratio of 1% is chosen for each mode. For simplicity, the plate is assumed to be simply-supported along all four edges, leading [9] to a lowest natural frequency of 2.741 Hz. This system has seven modes below 15 Hz and eleven below 22.5 Hz, including several quite closely-spaced ones; these two truncated modal models will be the ones used for the simulation results presented here. Three instruments are positioned at (0.3, 0.6), (0.6, 1.5) and (0.8, 1.2) m from the bottom left corner of the plate, and then iteratively moved, in steps of $0.0\bar{1}$ m, using either the method which seeks to minimize the largest HSV (based on $\mathbf{p}$) or that which minimizes the summed HSVs (based on $\mathbf{q}$). This will provide a clear illustration of the comparative performance of the two algorithms. (Many other cases are also reported in [38]; the interested reader is referred there for further details.)

The simply-supported rectangular plate has very simple mode shapes; their projections along either the x or y-axis are simply sinusoidal, with periods so as to give nodes at the edge supports. This has two implications. Firstly, the mode shape partial derivatives with respect to x and y, needed to

set up the matrix X in (8.1), are simple to calculate in closed-form. Secondly, the optimally non-interacting locations for a set of instruments on the plate are clearly along the edge nodal lines. This provides a means of testing the performance of the instrument placement algorithms: if either of the techniques does not position all instruments on the edges, it is clearly not achieving a global optimum.

As previously claimed, both of the HSV-based placement algorithms do indeed often produce very similar results. This is illustrated by Figures 9.1 and 9.2, which show the tracks followed by the three instruments for an 11-mode model as they are iteratively repositioned using the **p** method (Figure 9.1) and that based on **q** (Figure 9.2). The similarity between the instrument movements generated by the two algorithms in this case is clearly visible, and is confirmed by a comparison of the plots of decreasing maximal HSV and summed HSVs that the two methods produce. These are given as Figures 9.3 and 9.4.

It might therefore be concluded that the **q** method, being simpler and apparently producing results comparable to those obtained using **p**, is the preferred implementation in practice. However, examples are easy to construct where the **p** technique converges correctly to the edges of the plate, and yet the **q** method does not. For instance, Figures 9.5 and 9.6 give the results obtained for the same initial instrument locations as before, but with a plate model now truncated at seven modes rather than eleven. The method based on minimizing the summed HSVs now causes two of the instruments to move towards the center of the plate rather than the edges. The consequences for the Hankel singular values is shown in Figures 9.7 and 9.8: the **q** method causes virtually no change at all to the maximal HSV, and only a modest decrease in the summed HSVs. The **p** method, by contrast, reduces these observability quantities essentially to zero as before. The exact reason for the failure of the **q** algorithm to correctly position the instruments in this case is not clear at present, although it appears to be some form of local minimum property. The practical

implication *is* clear though: it is that the modest increase in computation required by the **p** method over that based on **q** is well worthwhile for the additional robustness it provides.

9.2 ASTREX Structure

The instrument placement techniques will now be applied to the ASTREX truncated modal model described in [39][40]. ASTREX consists of two major sections: a pivoting test article (Figure 9.9), and a vertical pedestal that supports the test article through an air-bearing system. The air bearing is leveled such that the test article points downwards from the horizontal by about 30°. The test article is designed to represent a space-based reflector system. The front section is attached to the large primary by a tripod support, and represents a secondary mirror; the rear section represents a tertiary reflector; it houses electronics and balances the secondary.

The modal model used here has 22 flexible modes, ranging in frequency from 3.71 Hz to 48.57 Hz, with an assumed damping ratio of 0.1% for all modes. The NASTRAN finite-element model used to generate the model possesses 375 node points, some of which are labeled in Figure 9.9. 36 nodes lie on the main reflector front face (Figure 9.10); for generality, all of these points will be considered to be candidate positions for instruments in the results that follow.

All of the results reported here for ASTREX were obtained using the instrument placement algorithm which is based on minimizing the largest Hankel singular value of the system. This is due to the difficulties sometimes observed when applying the summed-HSV technique to the plate model. In all cases, two instruments are initially positioned at random on the front face of the primary. The placement algorithm then iteratively moves the instruments, one step at a time, until the maximal HSV is reduced as much as possible. The differences between the various cases studied lie in the orientation of the two instrument sensing axes (either both along the x-axis, one along x and one along y, or both along z, i.e. normal to the plane of the primary), and in whether

or not there are any additional fixed disturbance sources present. Also, these disturbances were considered to act along either the x or the z axes.

The results obtained can be summarized as follows. Typically, an order of magnitude reduction was achieved in both the maximal Hankel singular value (directly) and the summed HSVs (indirectly) by repositioning instruments. For instance, the case of two x-axis instruments initially placed at nodes 68 and 86, i.e. along the outer edge of the primary truss, and no disturbance sources gives an initial maximal HSV of 3.534×10^{-4} and an HSV sum of 3.659×10^{-3}. After application of the placement algorithm, the instruments are positioned at nodes 131 and 164, along the inner edge of the primary, and the corresponding maximal and summed HSVs are 4.872×10^{-5} and 5.585×10^{-4}, respectively. Similarly, an x-axis instrument at node 90 and a y-axis one at node 80 were shifted by the algorithm to lie at nodes 108 and 164, respectively. The maximal HSV was correspondingly reduced from 6.690×10^{-3} to 6.811×10^{-5}, while the sum of the Hankel singular values dropped from 3.713×10^{-2} to 1.0173×10^{-3}. This reduction of nearly two orders of magnitude was one of the largest observed for any of the cases run.

Finally, the close connection between the frequency response of a system and its Hankel singular values implies that the new instrument placement technique should significantly reduce the peak magnitudes observed in cross-instrument responses. This is illustrated by Figure 9.11, which gives a typical ASTREX instrument Bode magnitude plot before (dashed) and after (solid) optimally repositioning the instruments. It can be seen that a reduction of about 30 dB has been achieved: given that this was obtained by the purely passive technique of shifting instrument locations, rather than by active feedback, it is really quite impressive.

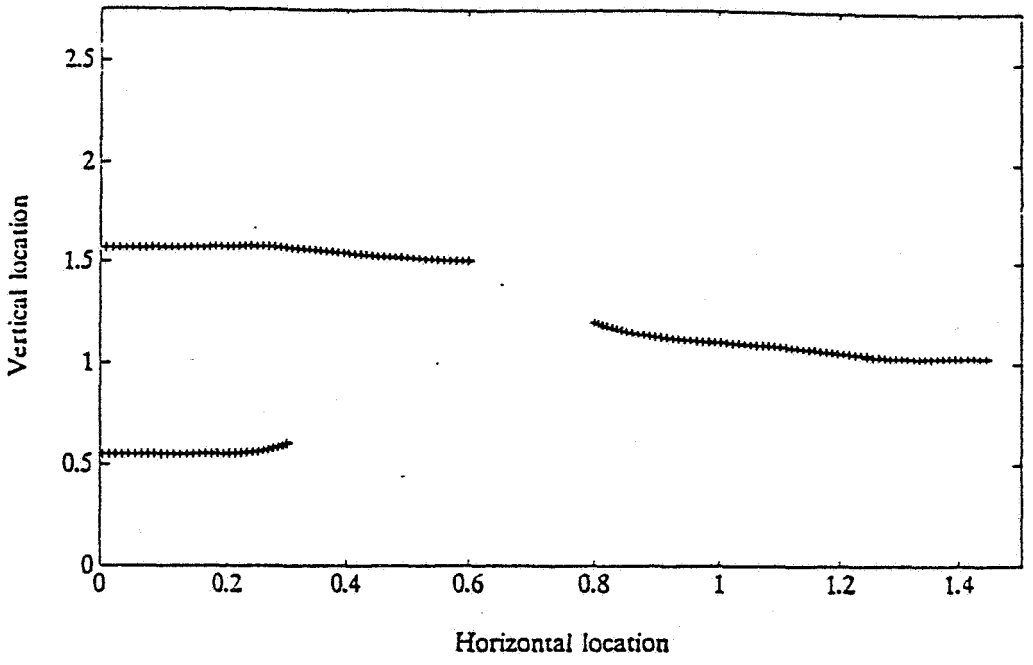

Figure 9.1. Evolution of instrument locations, p method.

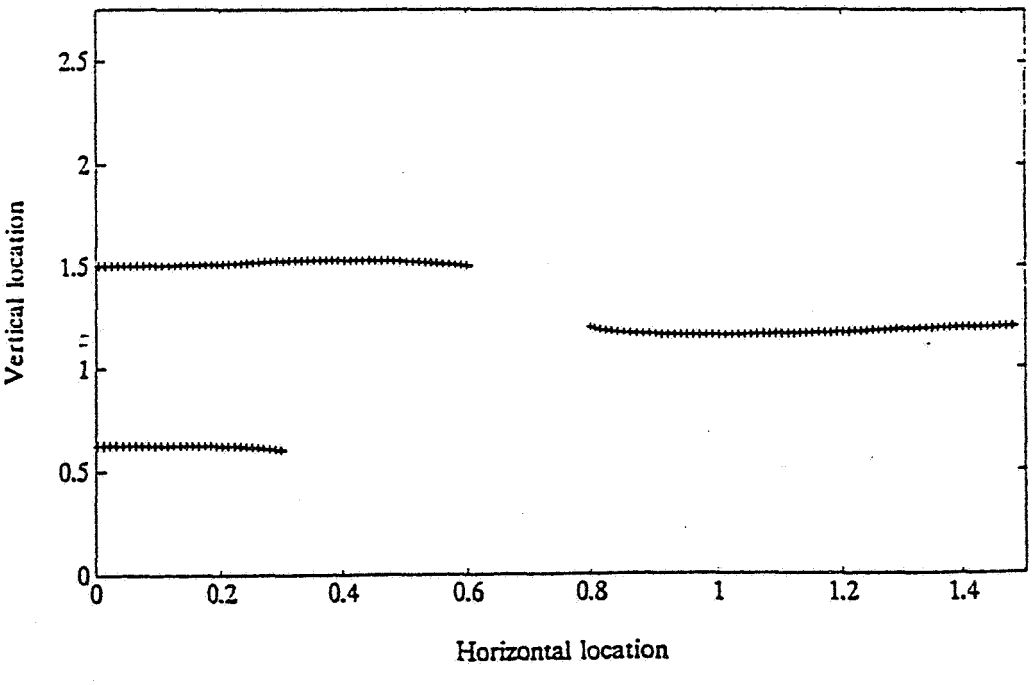

Figure 9.2. Evolution of instrument locations, q method.

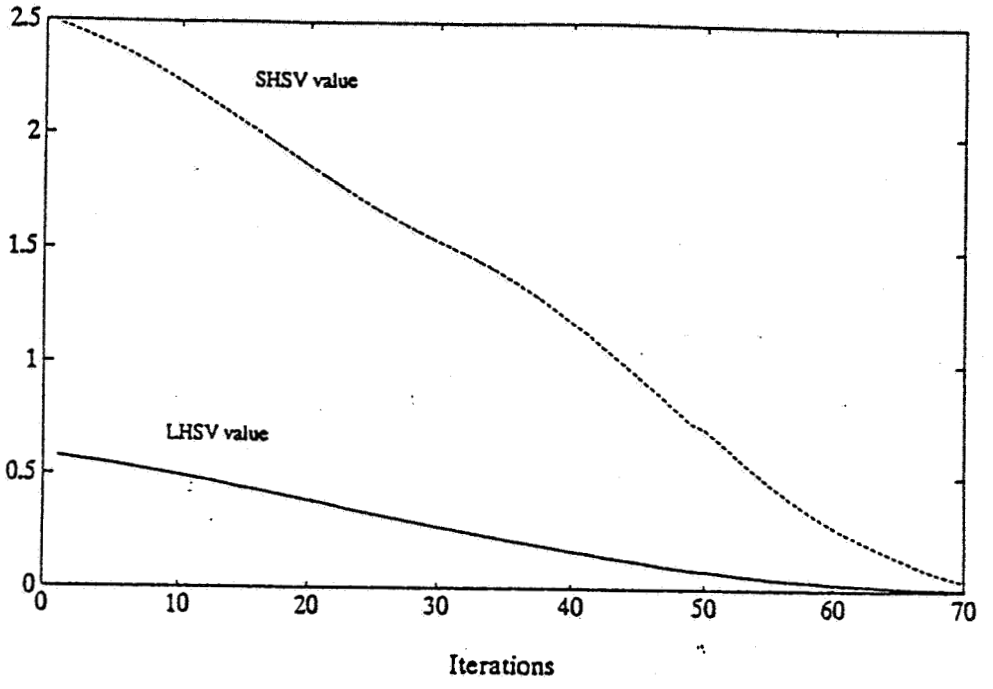

Figure 9.3. Evolution of HSVs, p method.

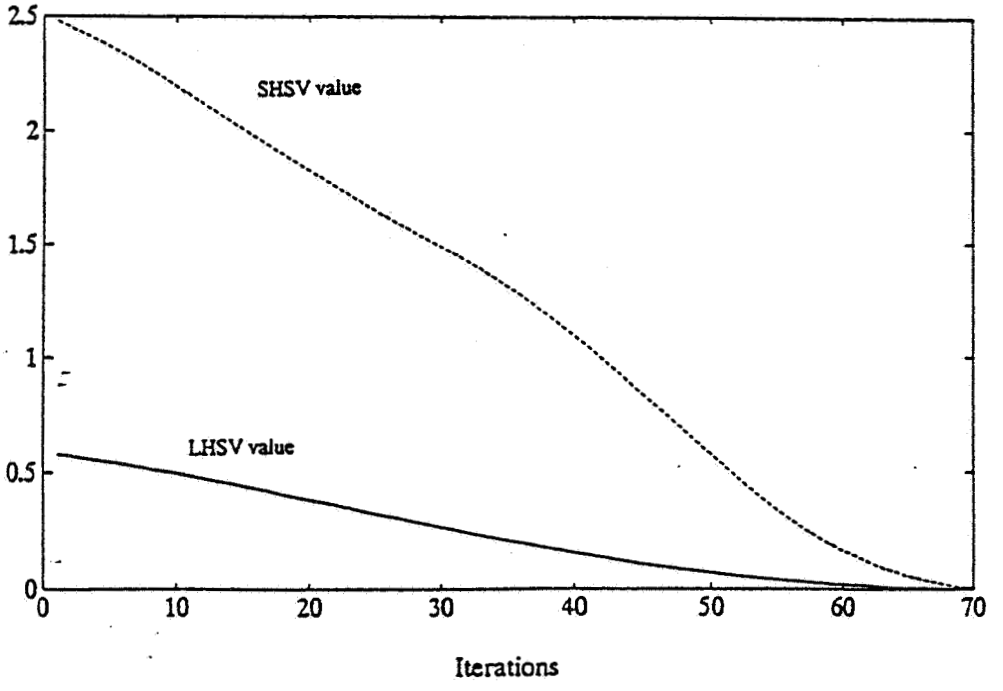

Figure 9.4. Evolution of HSVs, q method.

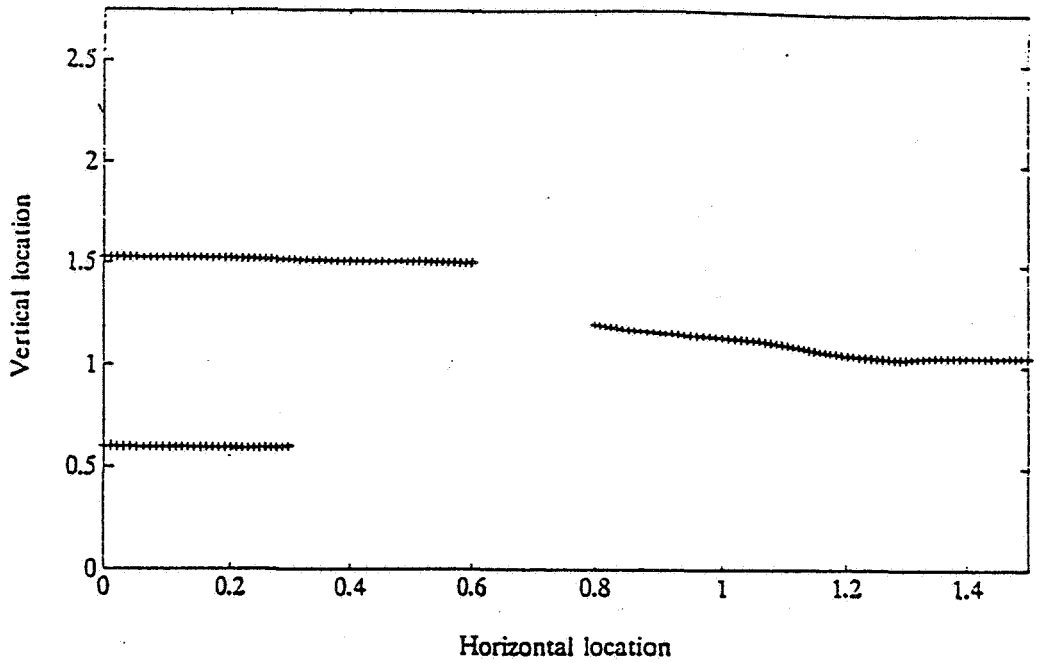

Figure 9.5. Evolution of instrument locations, p method.

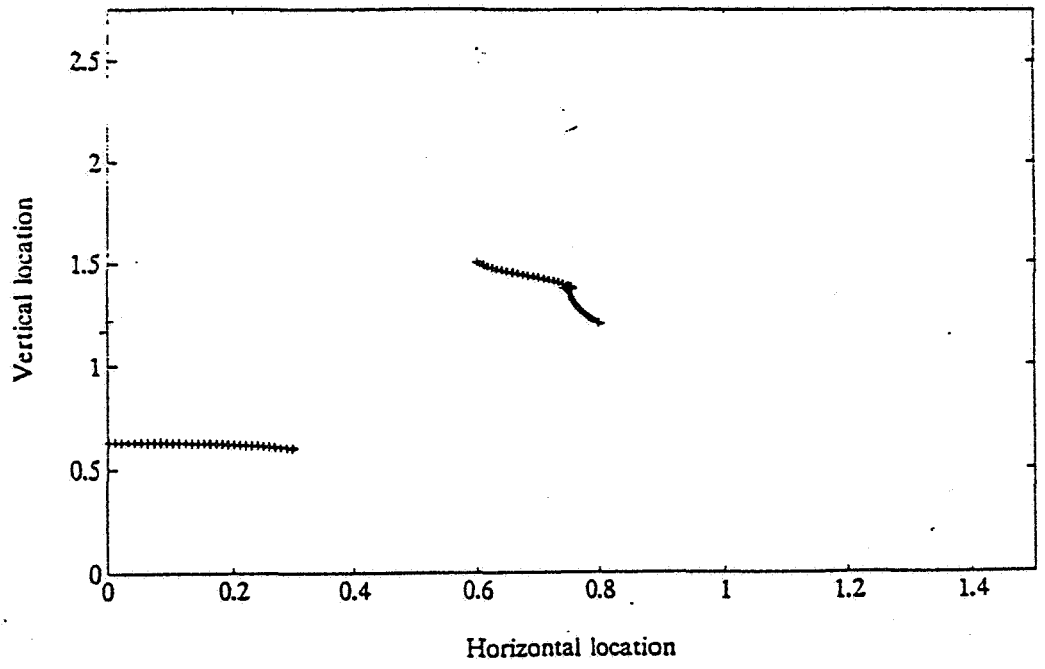

Figure 9.6. Evolution of instrument locations, q method.

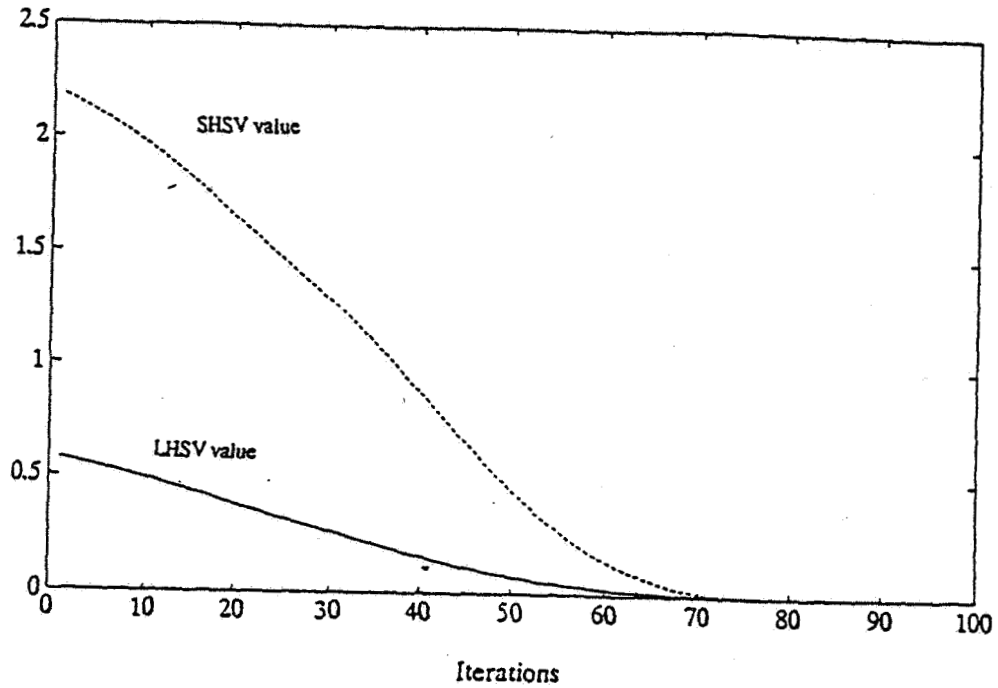

Figure 9.7. Evolution of HSVs, p method.

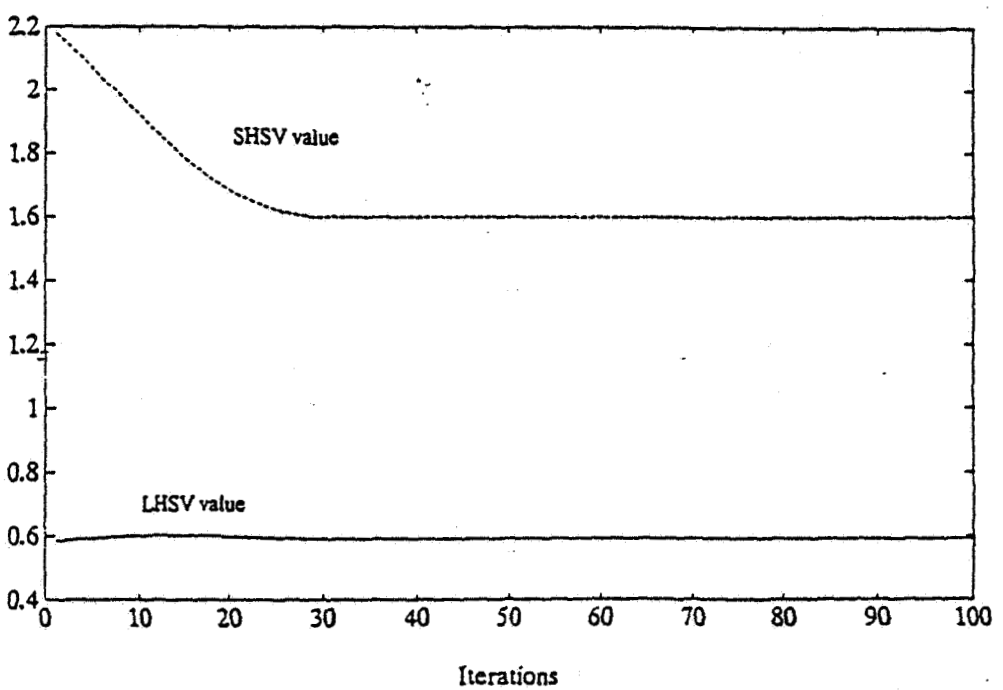

Figure 9.8. Evolution of HSVs, q method.

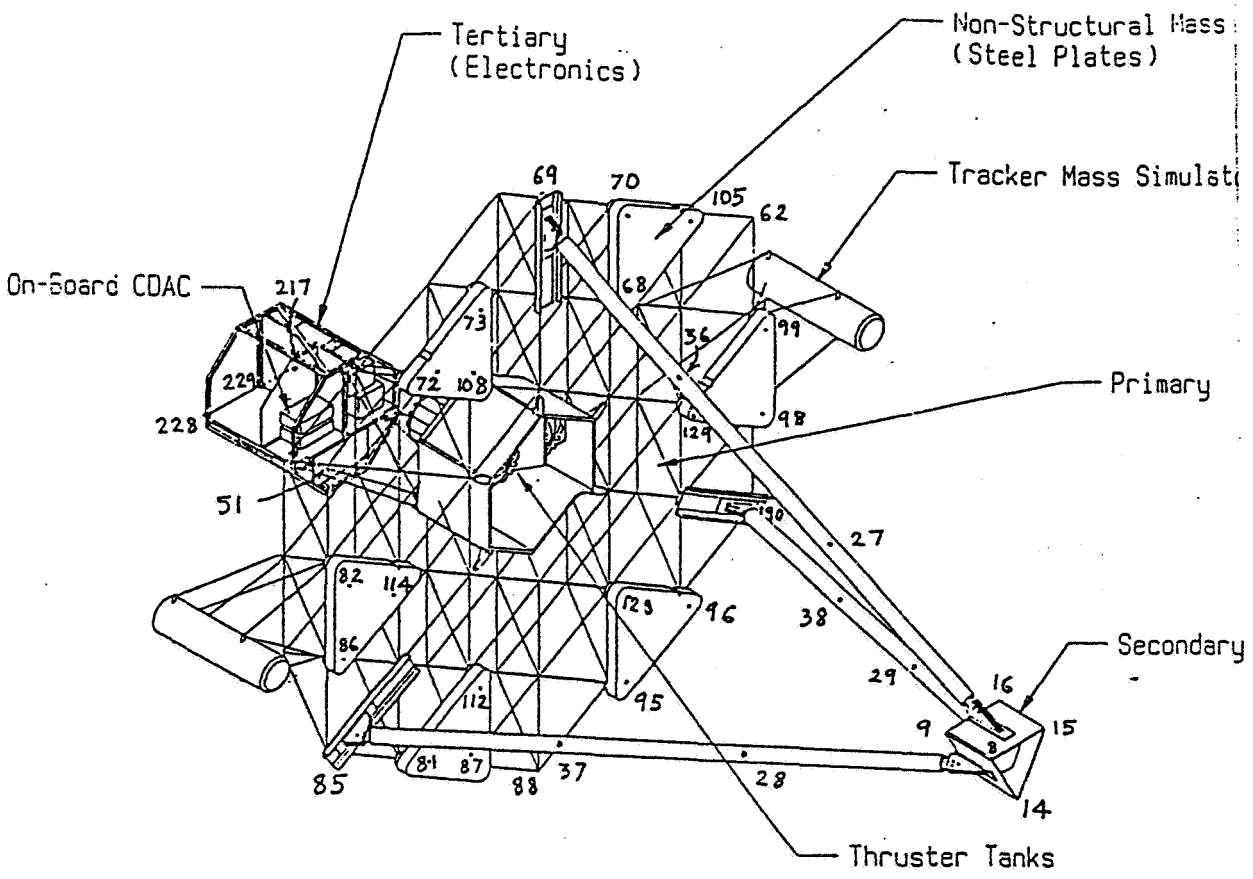

Figure 9.9. ASTREX test article.

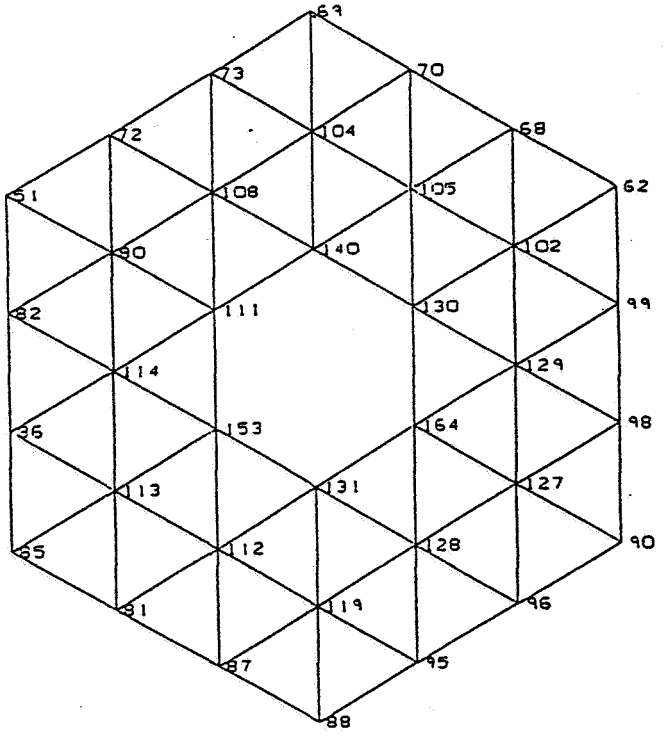

Figure 9.10. Node points, front primary face.

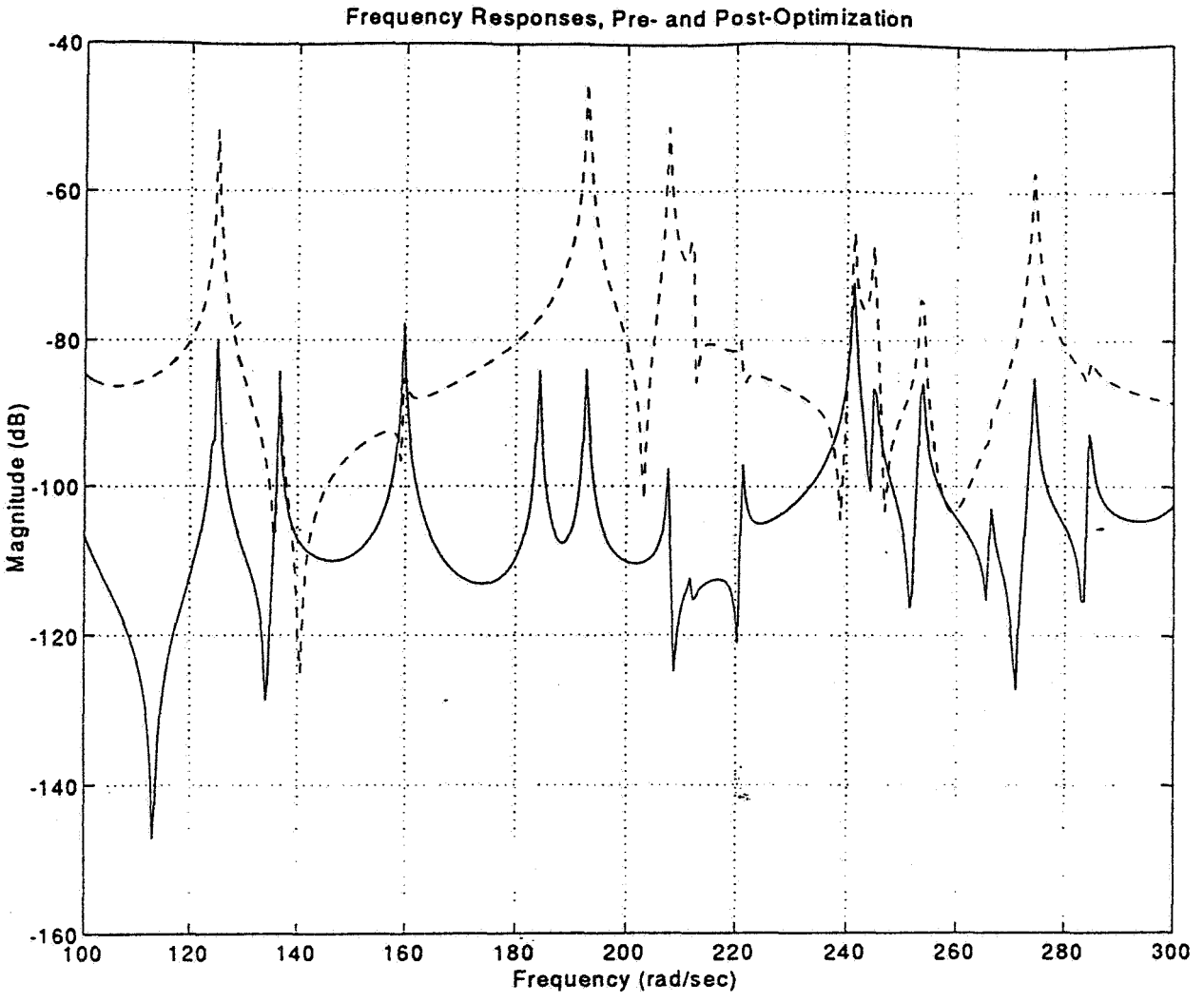

Figure 9.11. Frequency responses before and after placement.

10. Decentralized Control and Closed-Loop Grammians

The controllability and observability Grammians have been shown in the earlier portions of this report to be extremely useful quantities in the control of FSS. However, one limitation that they do possess is that they are inherently open-loop parameters. In particular, if control is to be implemented in a decentralized form, e.g. by means of a set of independent sensor/actuator pairs, the standard Grammians do not reflect the input/output mappings that exist between sensors and actuators. In order to facilitate the analysis of decentralized controllers for FSS, it is necessary instead to study the closed-loop Grammians that were introduced in [46]. This section defines these matrices, describs their properties, and shows how they can be applied to model reduction and sequential loop closing controller design problems for FSS with decentralized sensors and actuators.

In FSS control, model reduction is always necessary because of the limited capacity of on board computers. The reduction procedure can be fairly simple or rather complicated, depending on whether the control system is correlated or not. Simply speaking, two modes are uncorrelated, if there is no coupling term for these two modes in the controlability and observability grammians, and correlated otherwise. A more detailed way to measure how much two modes are correlated is by the ratio of the norm of the off-diagonal 2×2 blocks, to the square root of the product of the norms of the diagonal blocks. One simple way of this reduction is modal truncation, which simply discards higher order modes, since those modes are usually hard to excite and less accurate. A more complicated technique is so called balancing method, which transforms the system into a

coordinate where the modes are uncorrelated, then discards the modes with low modal cost [14]. It has been shown that for structures with light damping and widely spaced natural frequencies, the modal representation is almost identical to that of the balanced model [19][22][23].

However, for structures with repeated frequencies, especially, for FSS, where closely spaced modes are typical, this is not true. Ref. 16 shows that for these structures, balanced reduction generally gives far better results than simple modal reduction. Therefore, balancing should be carried out before model reduction of FSS control systems.

Here, it will be proved using closed-loop grammian, that an inner rate feedback loop, if designed appropriately, can greatly reduce the correlation of two closed modes. Therefore, this inner loop can balance FSS control system, and model reduction may be carried out directly sometimes without doing coordinate transformation. This result will be useful in FSS decentralized control design. It is especially useful in the design of high-authority/low-authority control (HAC/LAC), which is a special case of decentralized control.

Numerical examples will be given.

10.1 Closed-Loop Controllability Grammian

Suppose output feedback $\mathbf{u} = -K\mathbf{y}$ is applied to the system. The controllability grammian then becomes $W_c + \Delta W_c$, where

$$(A - BKC)(W_c + \Delta W_c) + (W_c + \Delta W_c)(A - BKC)^T + BB^T = 0 \qquad (10.1)$$

If relatively small gains are used, i.e. $\|BKC\| << \|A\|$, then, second-order terms of the form $BKC\Delta W_c$ can be neglected in (10.1). This, and the Lyapunov equation $AW_c + W_c A^T + BB^T = 0$, lead to the first-order approximation

$$A\Delta W_c + \Delta W_c + X = 0 \tag{10.2}$$

where

$$X = -BKCW_c - (BKCW_c)^T \tag{10.3}$$

is symmetric.

For FSS, A is block diagonal, so from (10.2) and (10.3) we have

$$A_{ij}\Delta W_{cij} + \Delta W_{cij} A_{ij}^T = -X_{ij} \tag{10.4}$$

where

$$X_{ij} = \begin{pmatrix} \alpha & \beta \\ \gamma & 0 \end{pmatrix} \tag{10.5}$$

$$A_{ij} = \omega_i \begin{pmatrix} -2\zeta_i & -1 \\ 1 & 0 \end{pmatrix} \tag{10.6}$$

The zero tērm in X_{ij} is resulted from the alternating zero raws in B.

Let

$$\Delta W_{cij} = \begin{pmatrix} p & q \\ r & s \end{pmatrix} \tag{10.7}$$

Then it can be shown, after some manipulation, that

$$p=\frac{(\omega_i^2-\omega_j^2)(-\gamma\omega_i+\beta\omega_j)+2\alpha\omega_i\omega_j(\zeta_i\omega_j+\zeta_j\omega_i)}{(\omega_i^2-\omega_j^2)^2+4\omega_i\omega_j(\zeta_i\omega_j+\zeta_j\omega_i)(\zeta_i\omega_i+\zeta_j\omega_j)} \tag{10.8}$$

$$q=\frac{-\alpha\omega_j(\omega_i^2-\omega_j^2)+2\omega_j(\zeta_i\omega_i+\zeta_j\omega_j)(-\gamma\omega_i+\beta\omega_j)}{(\omega_i^2-\omega_j^2)^2+4\omega_i\omega_j(\zeta_i\omega_j+\zeta_j\omega_i)(\zeta_i\omega_i+\zeta_j\omega_j)} \tag{10.9}$$

$$r=\frac{\alpha\omega_i(\omega_i^2-\omega_j^2)-2\omega_i(\zeta_i\omega_i+\zeta_j\omega_j)(-\gamma\omega_i+\beta\omega_j)}{(\omega_i^2-\omega_j^2)^2+4\omega_i\omega_j(\zeta_i\omega_j+\zeta_j\omega_i)(\zeta_i\omega_i+\zeta_j\omega_j)} \tag{10.10}$$

$$s=\frac{(\beta\omega_i-\gamma\omega_j)(\omega_i^2-\omega_j^2)+2\omega_i\omega_j(\alpha+2\beta\zeta_j+2\gamma\zeta_i)(\zeta_i\omega_i+\zeta_i\omega_i)}{(\omega_i^2-\omega_j^2)^2+4\omega_i\omega_j(\zeta_i\omega_j+\zeta_j\omega_i)(\zeta_i\omega_i+\zeta_j\omega_j)} \tag{10.11}$$

Therefore, simplifying, we have

$$\begin{aligned}\Delta W_{cij}=&\frac{1}{d_{ij}}((\omega_i^2-\omega_j^2)\begin{pmatrix}-\gamma\omega_i+\beta\omega_j & -\alpha\omega_j\\ \alpha\omega_i & \beta\omega_i-\gamma\omega_j\end{pmatrix}\\ &+(\zeta_i\omega_i+\zeta_j\omega_j)\begin{pmatrix}0 & 2\omega_j(-\gamma\omega_i+\beta\omega_j)\\ 2\omega_j(-\gamma\omega_i+\beta\omega_j) & 2\omega_i\omega_j(\alpha+2\beta\zeta_j+2\gamma\zeta_i)\end{pmatrix}\\ &+(\zeta_i\omega_j+\zeta_j\omega_i\begin{pmatrix}2\alpha\omega_i\omega_j & 0\\ 0 & 0\end{pmatrix})\end{aligned} \tag{10.12}$$

where $d_{ij}\triangleq 4\omega_i\omega_j(\zeta_j\omega_i+\zeta_i\omega_j)(\zeta_i\omega_i+\zeta_j\omega_j)+(\omega_j^2-\omega_i^2)^2$ is the same denominator term that appeared in the closed-form expression for the open-loop Grammian of FSS. From this denominator, and the fact that FSS usually have very small damping, we can see from (10.12) that the off-diagonal blocks are much smaller than the diagonal blocks. The diagonal blocks of ΔW_c simplify considerably: they are just:

$$\Delta W_{cii}=\frac{1}{4\zeta_i\omega_i}\begin{pmatrix}\alpha & 0\\ 0 & \alpha+4\zeta_i\beta\end{pmatrix}\approx\frac{\alpha}{4\zeta_i\omega_i}.I_2 \tag{10.13}$$

Therefore, for widely spaced lightly damped structures, ΔW_c is almost diagonal. Since in this kind of structures the open-loop Grammians are not correlated, we can know that when gains are small, the closed-loop Grammian will keep uncorrelated. On the contrary, for closed modes, there open-loop Grammian are correlated, as show in previous sections. When a control loop is applied, the Grammian perturbation is also not diagonal. Therefore, it is not clear how the resulting closed-loop is correlated.

In the next sub-section, it will be proved that the correlation between these close modes can be decreased under some conditions and increased under other conditions.

Consider a multi-input/multi-output (MIMO) control system with open-loop controllability W_c, when applied an inner single input/single output (SISO) collocated rate feedback control loop, as shown in Fig. 10.1, will have

$$X = -k(\mathbf{b}_I \mathbf{b}_I{}^T W_c + (\mathbf{b}_I \mathbf{b}_I{}^T W_c)^T) \tag{10.14}$$

where $\mathbf{b}_I$ is the inner loop n-vector. Considering (10.5), this gives

$$\begin{pmatrix} \alpha & \beta \\ \gamma & 0 \end{pmatrix} = -k\left(\begin{bmatrix} b_{Ii}{}^2 & 0 \\ 0 & 0 \end{bmatrix} W_{cij} + \begin{bmatrix} b_{Ii} b_{Ij} & 0 \\ 0 & 0 \end{bmatrix} W_{cji}\right) \tag{10.15}$$

For lightly damped widely-spaced modes, $\|W_{cij}\| << \|W_{cji}\|$, and W_{cji} is diagonal, β and γ are almost zero. However, for FSS, which have closed modes, it is not necessarily true.

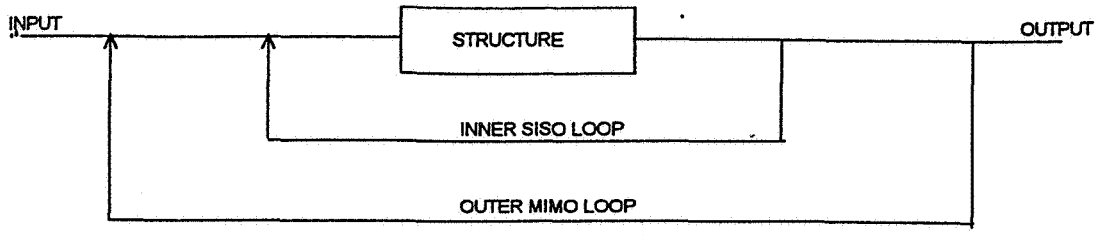

Fig.10.1 Block diagram of inner and outer loops.

10.2 Feedback Correlation Reduction for Close Modes

When model reduction is necessary, we hope that the correlation of modes are small, so that the model reduction can be carried out directly by modal truncation. Otherwise, coordinate transformations must be performed before model reduction. As mentioned in the last sub-section, for widely spaced, lightly damped modes, the correlation is always small, both in the open closed loop systems. But for close modes, the correlation is significant for open-loop systems, and not clear for closed loop systems. In this section, it will be shown that the correlation of close modes in closed loop system can be either decreases or increased. Conditions to reduce correlation of close modes will be given.

Theorem: If an inner rate feedback loop is applied to a control system as shown in Fig. 10.1, the correlation of two closed modes will decrease when β_{ij} and $\beta_{Iij} = b_{Ii} b_{Ij}$ have same sign, and increase otherwise.

The proof is carried out for three different cases. The first case is when the damping ratios are higher order small quantities than the difference of natural frequencies; the second case is when

the difference of natural frequencies is a higher order small quantity than the damping ratios; and the third is when the damping ratios and difference of natural frequencies are small quantities of the same order.

When damping ratio $\zeta_i \approx \zeta_j \to 0$:

From (5.5), when $\zeta_i, \zeta_j \to 0$ and ω_i, ω_j are separated

$$W_{cij} \approx \frac{\beta_{ij}}{(\omega_j{}^2 - \omega_i^2)} \begin{pmatrix} 0 & \omega_j \\ -\omega_i & 0 \end{pmatrix} \tag{10.16}$$

When $\omega_i = \omega_j$,

$$W_{cij} \approx \frac{\beta_{ij}}{2(\zeta_i + \zeta_j)\omega_i} . I_2 \tag{10.17}$$

In particular, the diagonal blocks are

$$W_{cii} \approx \frac{\beta_{ii}}{4\zeta_i \omega_i} . I_2 \tag{10.18}$$

Using (10.16), (10.18) and (10.15) gives:

$$\alpha = -k \frac{\beta_{Iij} \beta_{ii}}{2\zeta_j \omega_j} \tag{10.19}$$

$$\beta = \gamma \tag{10.20}$$

Substitute (10.20) into (10.12) and considering the small damping and the fact the frequencies we consider are close

$$\Delta W_{cij} \approx \frac{\alpha}{\omega_j^{\,2} - \omega_i^2}\begin{pmatrix} 0 & \omega_j \\ -\omega_i & 0 \end{pmatrix} \tag{10.21}$$

From (10.16), it can be found that the relative decrease of the norm of the (i, j) off-diagonal block is

$$\rho_{ij} = k\frac{\beta_{Iij}\beta_{ii}}{2\zeta_j\omega_j\beta_{ij}} \tag{10.22}$$

from which we can see that when β_{Iij} and β_{ij} have the same sign, the off-diagonal terms will always be reduced; otherwise, they will increase.

The relative decrease of the diagonal blocks can be found from (10.18) and (10.12) as

$$\rho_{ii} = k\frac{\beta_{Iii}}{2\zeta_j\omega_j} \tag{10.23}$$

From (10.22) and (10.23), it can be seen that the condition for the decrease of the off-diagonal blocks to be faster than that of the diagonal blocks is

$$\frac{\|\beta_{Iij}\beta_{ii}\|\|\beta_{Iij}\beta_{jj}\|}{\|\beta_{ij}\|\|\beta_{ji}\|} > \beta_{Iii}\beta_{Ijj} \quad \text{or} \quad \|\beta_{ii}\|\|\beta_{jj}\| > \|\beta_{ij}\|\|\beta_{ji}\| \tag{10.24}$$

which by the Triangle Inequality, is always satisfied.

When $\omega_i \to \omega_j$:

From (10.17) (10.18) and (10.15),

$$\alpha = \frac{-k}{2\zeta_j \omega_j}(\beta_{ij}\beta_{Iii} + \beta_{jj}\beta_{Iij}) \tag{10.25}$$

$$\beta = \gamma = 0 \tag{10.26}$$

The relative decrease of the off-diagonal blocks are

$$\rho_{ij} = \frac{k}{2\zeta_j \omega_j}\frac{\beta_{ij}\beta_{Iii} + \beta_{jj}\beta_{Iij}}{\beta_{ij}} \tag{10.27}$$

Those of the diagonal blocks are , from (10.10) and (10.23)

$$\rho_{ii} = \frac{k}{2\zeta_i \omega_i} 2\beta_{Iii} \tag{10.28}$$

For off-diagonal blocks to decrease faster than the diagonal blocks requires

$$\left\| \frac{k}{2\zeta_i \omega_i} 2b_{Ii}^2 \right\| \left\| \frac{k}{2\zeta_j \omega_j} 2b_{Ij}{}^2 \right\| < \left\| \frac{k}{2\zeta_j \omega_j} \frac{\beta_{ij}\beta_{Iii} + \beta_{jj}\beta_{Iij}}{\beta_{ij}} \right\| \left\| \frac{k}{2\zeta_i \omega_i} \frac{\beta_{ij}\beta_{Ijj} + \beta_{jj}\beta_{Iij}}{\beta_{ij}} \right\|$$

Rearranging gives

$$4 < \left\| 1 + \frac{\beta_{jj} b_{Ij}}{\beta_{ij} b_{Ii}} \right\| \left\| 1 + \frac{\beta_{ii} b_{Ii}}{\beta_{ij} b_{Ij}} \right\| \tag{10.29}$$

Since $\left\| \frac{\beta_{ii} b_{Ii}}{\beta_{ij} b_{Ij}} \right\| \left\| \frac{\beta_{jj} b_{Ij}}{\beta_{ij} b_{Ii}} \right\| = \frac{\|\beta_{ii}\| \|\beta_{jj}\|}{\|\beta_{ij}\|^2} > 1$, if β_{ij} and $\beta_{Iij} = b_{Ii} b_{Ij}$ have same sign, which is the condition required in the previous case, (10.29) is always satisfied.

When damping ratio and difference of natural frequencies are of same order:

Let $\omega_i = \omega$, $\omega_j = (1+\varepsilon)\omega$, $\zeta_i = \zeta_j = \zeta$, then, from (5.5)

$$W_{cij} \approx \frac{\beta_{ij}}{D_{ij}} \begin{pmatrix} 2\zeta & \varepsilon \\ -\varepsilon & 2\zeta \end{pmatrix} \tag{10.30}$$

where $D_{ij} \approx 4\omega^4(\varepsilon^2 + 4\zeta^2)$

$$\Delta W_{cij} = \frac{2\omega^3}{D_{ij}} \begin{pmatrix} \varepsilon(\gamma-\beta)+2\alpha\zeta & 2\zeta(\beta-\gamma)+\alpha\varepsilon \\ -2(\beta-\gamma)-\alpha\varepsilon & \varepsilon(\gamma-\beta)+2\alpha\zeta \end{pmatrix} \tag{10.31}$$

From (10.18), (10.30) and (10.14)

$$\alpha = -k\frac{2\omega^3}{D}((\beta_{ij}\beta_{Iii} + \beta_{jj}\beta_{Iij})2\zeta \tag{10.32}$$

$$\beta = \gamma = -k\frac{2\omega^3}{D}\beta_{ij}\beta_{Iii}\varepsilon \tag{10.33}$$

(10.31) then becomes

$$\Delta W_{cij} = \frac{2\omega^3}{D_{ij}} \begin{pmatrix} 2\alpha\zeta & \alpha\varepsilon \\ -\alpha\varepsilon & 2\alpha\zeta \end{pmatrix} \tag{10.34}$$

The relative decrease of the off-diagonal blocks is, then,

$$\rho_{ij} = \frac{k2\omega^3\varepsilon}{D_{ij}} \cdot \frac{\beta_{ij}\beta_{Iii} + \beta_{jj}\beta_{Iij}}{\beta_{ij}} \tag{10.35}$$

Those of the diagonal blocks are , from (10.18) and (10.12)

$$\rho_{ii} = \frac{k}{D_{ij}} 4\omega^3 \varepsilon b_{Ii}^2 \tag{10.36}$$

For the off-diagonal blocks to decrease faster than the diagonal blocks requires

$$\left\| \frac{k}{D_{ij}} 4\omega^3 \varepsilon \beta_{Iii} \right\| \left\| \frac{k}{D_{ij}} 4\omega^3 \varepsilon \beta_{Ijj} \right\| < \left\| \frac{k2\omega^3\varepsilon}{D_{ij}} \cdot \frac{\beta_{ij}\beta_{Ijj} + \beta_{iij}\beta_{Iij}}{\beta_{ij}} \right\| \left\| \frac{k2\omega^3\varepsilon}{D_{ij}} \cdot \frac{\beta_{ij}\beta_{Iii} + \beta_{jj}\beta_{Iij}}{\beta_{ij}} \right\|$$

Rearranging gives the same result as (10.24), hence the same conclusion.

10.3 Application To FSS Decentralized Control Design

Application to general FSS decentralized control system design

A FSS decentralized control system consists of several independent loops, some of which are SISO, some MIMO. The design of these loops can be conducted, one by one, independently.

One problem, though, is that when each control loop is applied, the resulting closed-loop will have different controllability and observability from that before the loop is applied. Although the perturbation incurred by each loop may be small, when several loops are applied, the perturbation can be significant.

However, with the formulas derived in Section 10.1, the controllability and observability of closed-loop can be found when each loop is applied.

Another changing property, when each loop is applied, is the correlation of different modes. As can be seen from Section10.2, the correlation of closed modes decreases under certain conditions and increases sometimes. This result will be useful in FSS decentralized control design.

FSS often have close modes, between which there are significant correlation. Therefore, the model reduction can not be done directly. However, if the result of 10.3 is adopted in design, the correlation of closed modes can be reduced, and model reduction can often be carried out directly.

The procedure is:

1. Group one of the MIMO loop with several SISO loops, which satisfy the condition for decreasing the correlation of the closed modes.

2. Then if the gains are appropriate, the correlation could be neglected and model reduction can be done by simply discarding those modes with small modal cost.

3. After the design of this group of loops, form another group in the same way and carry out design.

Application to high-authority/low-authority control (HAC/LAC)

One example of decentralized control is HAC/LAC [19]. The low damping of FSS makes control design much more difficult. The difficulty lies in the fact that once the modes are excited, it takes considerable time to go to rest, and since the open loop poles are very close to imaginary axis, it is easily destabilized by spillover of unmodelled modes. One way to overcome this is using HAC/LAC. In this approach, an inner loop (LAC) is installed to augment the damping then design the outer loop (HAC) for desired performance.

From the conclusions of previous sections, this inner loop not only can increases the damping, but also can reduces the correlation of controllability and observability grammians. Therefore, if the inner loop is appropriately designed, the resulting system will be balanced and of relatively high damping. The model reduction can then be carried out directly, also the HAC design.

The design can be carried out following this procedure:

1. Find the close frequencies which needs to be balanced.

2. Calculate β_{ij} for both B and C matrix.

3. Find the positions where $b_{Ii}b_{Ij}$ have same sign with β_{ij} for both B and C.

4. For best effect, find the position where $\frac{\|\beta_{ii}\|\|\beta_{jj}\|}{\|\beta_{ij}\|^2}$ has values as large as possible.

5. Give a gain k and calculate the correlation. When the correlation is not small enough, increase k, until it is small enough.

6. Find the reduced order modes by eliminating the modes with small cost.

7. Design the HAC for the reduced model.

10.4 Numerical Examples

A uniform cantilever beam model with the natural frequency of mode 4 artificially shifted to make modes 3 4 close is used to calculate the correlation of W_c and W_o for different cases. We keep modes 1 2 unchanged and observe the correlation of modes 3 4. An HAC/LAC is used to control the system, with HAC two input two output.

Figure 10.2 shows the mode shapes of the first four modes.

Figure 10.3 shows the correlation for different k. The two actuators of HAC are installed at L/2 and L from the fixes end, and two sensors at 0.1L and 0.975L. If the LAC loop is placed at 3L/4, we can find that $\beta_{34} < 0, \beta_{I34} < 0$. It can be seen that the correlation is drastically reduced.

Figure 10.4 shows the correlation for W_o, when the sensor are at 0.1L and 0.975L.

If the outer loop is a collocated loop with sensors and actuator at L/2 and L, the correlation can also be significantly reduced. Figure 10.5 shows the correlation for W_o, when the sensors are at L/2 and L, which is a collocated case.

However, a poor choice of inner loop may even increase the correlation. Figure 10.6 shows with the same outer loop, and the inner loop installed at L/4, which makes $\beta_{34} > 0$ .It can be seen that the correlation is not decreased but rather increased. To avoid this, we need to make sure that β_{34} and β_{I34} have same sign.

One important property of this method is that the inner loop will never increase the low correlation between widely separated modes. Figure 10.7 shows that with these feedback, the correlation between widely spaced modes 1 and 2 are indeed changed very little.

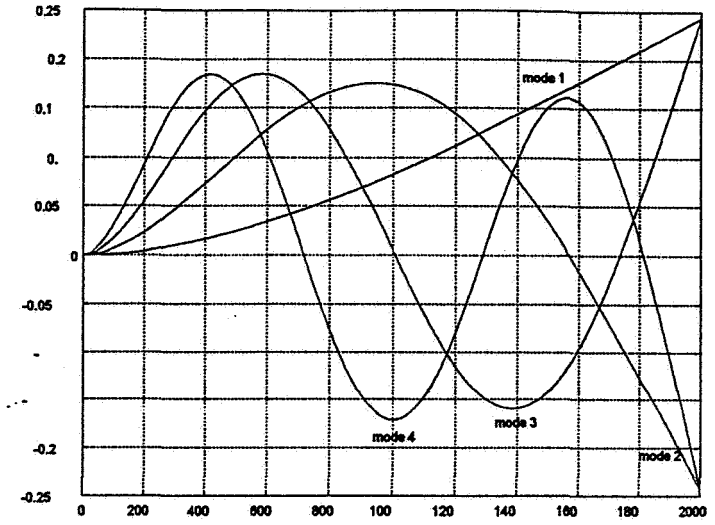

Fig10.2 Mode shapes

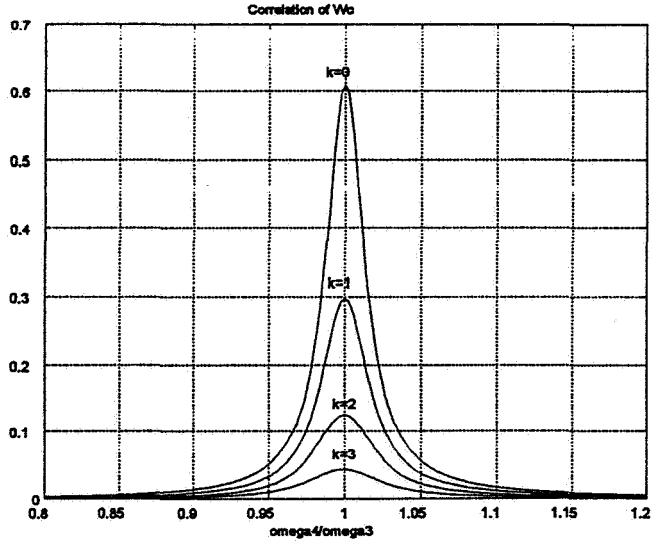

Fig 10.3 Controllability correlation for modes 3 and 4

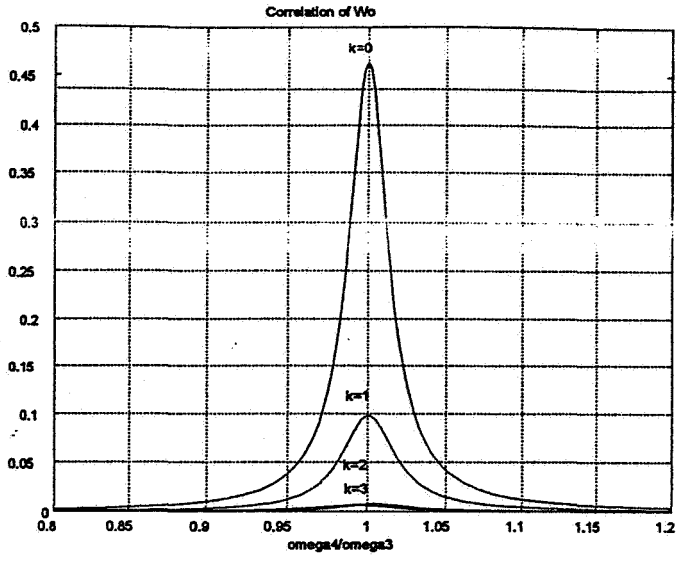

Fig 10.4 Observability correlation for modes 3 and 4

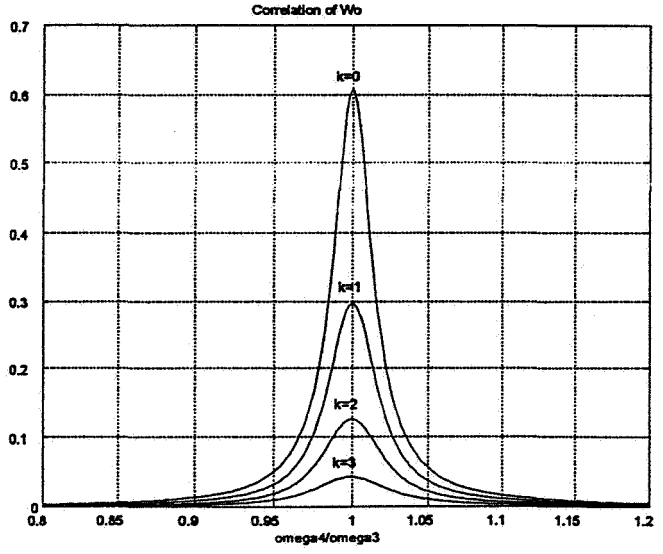

Fig 10.5 Observability correlation for modes 3 and 4

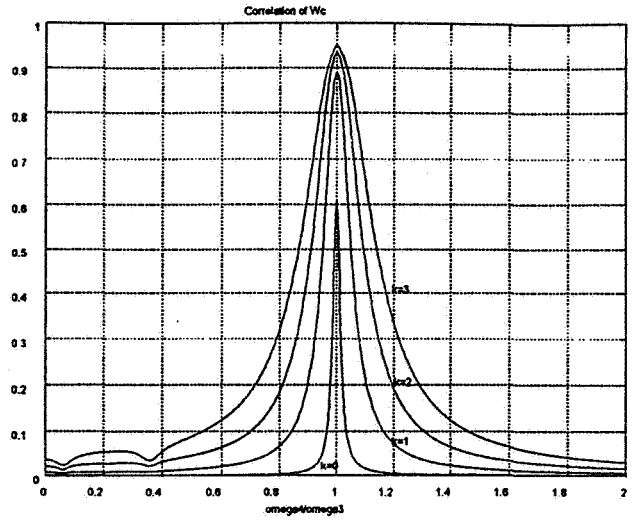

Fig 10.6 Controllability correlation for modes 3 and 4

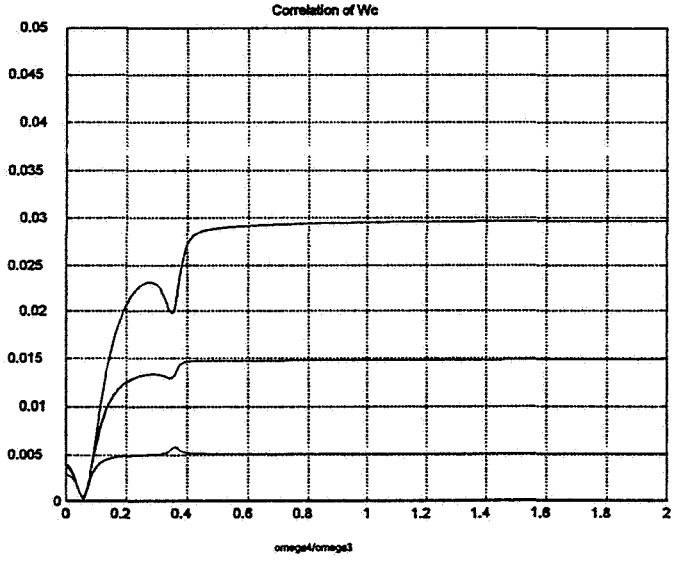

Fig 10.7 Controllability correlation for modes 1 and 2

11. Conclusions

The first part of this report analyzed the extreme sensitivity to sensor and actuator position that can occur for the transmission zeros of non-collocated flexible structures. This sensitivity was quantified directly in terms of a pair of new zeros condition numbers that were defined here. These variables help to explain the fundamental differences that arise in zeros sensitivity in the collocated and non-collocated cases. They also provide insight into the effects of small actuator shifts on the resulting closed-loop poles, and guidance as to how to shift non-collocated sensors and actuators so as to make the resulting zeros as damped as possible.

The report then described two computationally efficient techniques for the related problem of positioning instruments on a flexible structure so as to minimize the disturbance effects of the slewing of one instrument on the pointing performance of the others. Both approaches were based on perturbation methods involving the closed-form Hankel singular values of flexible structures. Iterating over all instruments led to a final set of highly non-interacting instrument locations. These methods were illustrated by application to a uniform simply-supported plate, as an example of a continuous structure, as well as to the discrete ASTREX truss structure. Both these examples demonstrated the improvement in performance that is achievable by the purely passive technique of repositioning instruments.

Finally, it was pointed out that the control of flexible space structures (FSS) must often be performed by means of a set of decentralized, i.e. independent, sensors and actuators. This constraint on the structure of the feedback gain matrix implies that decentralized controllers will generally possess lower performance than that of a centralized controller. For instance, there may exist closed-loop poles which can be shifted by centralized feedback but not by decentralized control. The final part of the report addressed the question of designing efficient decentralized controllers for FSS. One factor which must be borne in mind in this analysis is that the controllability and observability Grammian matrices which are usually studied are inherently open-

loop quantities; they therefore do not reflect any decentralized structure present in the controller. In order to overcome this problem, the new *closed-loop Grammians* were introduced, and their utility in the analysis of decentralized FSS controllers demonstrated. In particular, they were shown to lead to a natural technique for performing a sequential loop-closing form of controller design, based on closing the single input/single output feedback loop between each decentralized sensor/actuator pair in turn.

Acknowledgements

The following students contributed to the work reported here: Charles Inniss, Kelly McInerney, Jiafan Xu, Wang Fenfei, Xiao Cheng, Jianguo Wu and the late Masoud Mostarshedi. Their efforts are gratefully acknowledged.

References

[1] F.M. Fleming and E.F. Crawley, 'The Effect of Structure, Actuator and Sensor on the Zeros of Controlled Structures', *MIT Space Engineering Research Center Report 18-90* (1990).

[2] T.W.C. Williams, 'Transmission Zeros of Non-Collocated Flexible Structures: Finite-Dimensional Effects', *Proc. AIAA Dynamics Specialists Conference (AIAA CP923)*, pp. 356-364, Dallas, Texas, Apr. 1992.

[3] C.S. Inniss, *Sensitivity Analysis of the Transmission Zeros of Non-Collocated Flexible Structures*, M.S. Thesis, University of Cincinnati, Dec. 1992.

[4] T.W.C. Williams, 'Transmission Zero Bounds for Large Space Structures, with Applications', *Journal of Guidance, Control, and Dynamics*, Vol. 12, pp. 33-38, 1989.

[5] T.W.C. Williams, 'Model Order Effects on the Transmission Zeros of Flexible Space Structures', *Journal of Guidance, Control, and Dynamics* , Vol. 15, pp. 540-543, 1992.

[6] T.W.C. Williams and J.N. Juang, 'Sensitivity of the Transmission Zeros of Flexible Space Structures', *Journal of Guidance, Control, and Dynamics*, Vol. 15, pp. 368-375, 1992.

[7] G.D. Martin and A.E. Bryson, 'Attitude Control of a Flexible Spacecraft', *Journal of Guidance and Control*, Vol. 3, pp. 37-41, 1980.

[8] T.W.C. Williams, 'Constrained Modes in Control Theory: Transmission Zeros of Uniform Beams', *Journal of Sound and Vibration*, Vol. 156, pp. 170-177, 1992.

[9] R.R. Craig, *Structural Dynamics*, New York: Wiley, 1981.

[10] S.M. Joshi, *Control of Large Flexible Space Structures*, Berlin: Springer-Verlag, 1989.

[11] G.W. Stewart and J. Sun, *Matrix Perturbation Theory*, New York: Academic Press, 1990.

[12] J.H. Wilkinson, *The Algebraic Eigenvalue Problem*, Oxford: Oxford University Press, 1965.

[13] G.W. Stewart, *Introduction to Matrix Computations*, New York: Academic Press, 1973.

[14] B.C. Moore, 'Principal Component Analysis in Linear Systems: Controllability, Observability, and Model Reduction', *IEEE Transactions on Automatic Control*, Vol. 26, Feb. 1981, pp. 17-32.

[15] T.W.C. Williams and M. Mostarshedi, 'Model Reduction Results for Flexible Space Structures', 5th NASA/DoD Controls-Structures Interaction Technology Conference, Lake Tahoe, NV, Mar. 1992.

[16] W.K. Gawronski and T.W.C. Williams, 'Model Reduction for Flexible Space Structures', *Journal of Guidance, Control, and Dynamics*, Vol. 14, Jan.-Feb. 1991, pp. 68-76.

[17] M.J. Balas, 'Trends in Large Space Structure Control Theory: Fondest Hopes, Wildest Dreams', *IEEE Transactions on Automatic Control*, Vol. 27, 1982, pp. 522-535.

[18] T.W.C. Williams, 'Closed-Form Grammians and Model Reduction for Flexible Space Structures', *IEEE Transactions on Automatic Control*, Vol. 35, Mar. 1990, pp. 379-382.

[19] R.E. Skelton, R. Singh and J. Ramakrishnan, 'Component Model Reduction by Component Cost Analysis', *Proc. AIAA Guidance, Navigation and Control Conference*, Aug. 1988, pp. 264-274.

[20] R.H. Bartels and G.W. Stewart, 'Solution of the Matrix Equation AX + XB = C', *Communications ACM*, 1972, pp. 820-826.

[21] E.A. Jonckheere and L.M. Silverman, 'Singular Value Analysis of Deformable Systems', *Proc. 20th IEEE Conference on Decision and Control*, Dec. 1981, pp. 660-668.

[22] C.Z. Gregory, 'Reduction of Large Flexible Spacecraft Models using Internal Balancing Theory', *Journal of Guidance, Control, and Dynamics*, Vol. 7, Nov.-Dec. 1984, pp. 725-732.

[23] E.A. Jonckheere, 'Principal Component Analysis of Flexible Systems - Open-Loop Case', *IEEE Transactions on Automatic Control*, Vol. 29, Dec. 1984, pp. 1095-1097.

[24] T.W.C. Williams and X. Cheng, 'Degrees of Controllability and Observability for Close Modes of Flexible Space Structures', submitted for publication, *IEEE Transactions on Automatic Control.*

[25] J.A. de Abreu-Garcia and F.W. Fairman, 'A Note on Cross-Grammians for Orthogonally Symmetric Realizations', *IEEE Transactions on Automatic Control*, Vol. 31, Sept. 1986, pp. 866-868.

[26] A.J. Laub, 'Computation of "Balancing" Transformations', *Proc. Joint Automatic Control Conference*, Aug. 1980.

[27] G.H. Golub and C.F. Van Loan, *Matrix Computations*, Baltimore: Johns Hopkins, 1983.

[28] G.J. Bierman, *Factorization Methods for Discrete Sequential Estimation*, New York: Academic, 1977.

[29] T.W.C. Williams, 'Identification of Large Space Structures: A Factorization Approach', *Journal of Guidance, Control, and Dynamics*, Vol. 10, July-Aug. 1987, pp. 466-473.

[30] T.W.C. Williams, 'Computing the Transmission Zeros of Large Space Structures', *IEEE Transactions on Automatic Control*, Vol. 34, Jan. 1989, pp. 92-94.

[31] M. Mostarshedi, *Model Reduction of Flexible Structures using Subsystem Balancing and the Closed Form of the Grammians*, M.S. Thesis, University of Cincinnati, Dec. 1991.

[32] P.G. Maghami and S.M. Joshi, 'Sensor/Actuator Placement for Flexible Space Structures', *Proc. American Control Conference*, June 1990, pp. 1941-1948.

[33] T.W.C. Williams, 'Transmission Zeros and High-Authority/Low-Authority Control of Flexible Space Structures', *Journal of Guidance, Control, and Dynamics*, Vol. 17, Jan.-Feb. 1994, pp. 170-174.

[34] J.F. Doyle, *Wave Propagation in Structures*, New York:Springer-Verlag, 1989.

[35] T. Kailath, *Linear Systems*, Englewood Cliffs: Prentice-Hall, 1980.

[36] R.E. Skelton, P.C. Hughes and H.B. Hablani, 'Order Reduction for Models of Space Structures Using Modal Cost Analysis', *Journal of Guidance, Control, and Dynamics*, Vol. 5, July-Aug. 1982, pp. 351-357.

[37] B. Schafer and H. Holzach, 'Identification and Model Adjustment of a Hanging Plate Designed for Structural Control Experiments', *Proc. 2nd Int. Symp. Str. Contr.*, Waterloo, Canada, 1985.

[38] K. McInerney, *Near-Optimal Collocated Instrument Placement for a Simply-Supported Flexible Rectangular Plate*, M.S. Mini-Thesis, University of Cincinnati, May 1993.

[39] V. Rao, K. Ngo, J. Berg and A. Das, 'Derivation of Reduced Order Models for Large Flexible Structures', AIAA Guidance, Navigation and Control Conference, New Orleans, Louisiana, Aug. 1991.

[40] N.S. Abhyankar and J.L. Berg, 'ASTREX Model Information: Supplement to astabcd.mat File', Phillips Laboratory Internal Report, Aug. 15, 1991.

[41] K. Choe and H. Baruh, 'Actuator Placement in Structural Control', *Journal of Guidance, Control, and Dynamics*, Vol. 15, Jan.-Feb. 1992, pp. 40-48.

[42] K.B. Lim, 'Method for Optimal Actuator and Sensor Placement for Large Flexible Structures', *Journal of Guidance, Control, and Dynamics*, Vol. 15, Jan.-Feb. 1992, pp. 49-57.

[43] F.R. Gantmacher, *The Theory of Matrices*, New York: Chelsea, 1959.

[44] J.N. Aubrun, 'Theory of the Control of Structures by Low-Authority Controllers', *Journal of Guidance and Control*, Vol. 3, No. 5, 1980, pp. 441-451.

[45] J.N. Aubrun, M.J. Ratner and M.G. Lyons, 'Structural Control for a Circular Plate', *Journal of Guidance, Control, and Dynamics*, Vol. 7, No. 5, 1984, pp. 535-545.

[46] T.W.C. Williams and J. Xu, 'Closed-Loop Grammians of Flexible Space Structures', *Proc 33rd IEEE Conference on Decision and Control*, Dec. 1994.